# Title: Intermediate-Phase Engineering via Dimethylammonium Cation Additive for Stable Perovskite Solar Cells

*David P. McMeekin,[1,2,3§*] Philippe Holzhey,[1§] Sebastian O. Fürer,[2,3] Steven P. Harvey,[4] Laura T. Schelhas[5] James M. Ball,[1]* Suhas Mahesh,[1] Seongrok Seo,[1] *Nicholas Hawkins,[6] Jianfeng Lu,[2,3] Michael B. Johnston,[1] Joseph J. Berry,[4] Udo Bach[2,3*] and Henry J. Snaith[1*]*

[1] Clarendon Laboratory, Department of Physics, University of Oxford, Parks Road, Oxford, OX1 3PU, United Kingdom

[2] Department of Chemical Engineering, Monash University, Victoria 3800, Australia

[3] ARC Centre of Excellence for Exciton Science, Monash University, Victoria 3800, Australia

[4] Material Science Center, National Renewable Energy Laboratory, Golden, CO 80401, USA

[5] Applied Energy Programs, SLAC National Accelerator Laboratory, Menlo Park, California 94025, USA

[6] Chemistry and Nanoscience Center, National Renewable Energy Laboratory, Golden, CO 80401, USA

[7] Department of Zoology, University of Oxford, South Parks Road, Oxford, OX1 3PS, UK

[§] These authors contributed equally to this work.

[*] Corresponding author E-mail: David.McMeekin@physics.ox.ac.uk

Udo.Bach@monash.edu, henry.snaith@physics.ox.ac.uk

## Supplementary Information

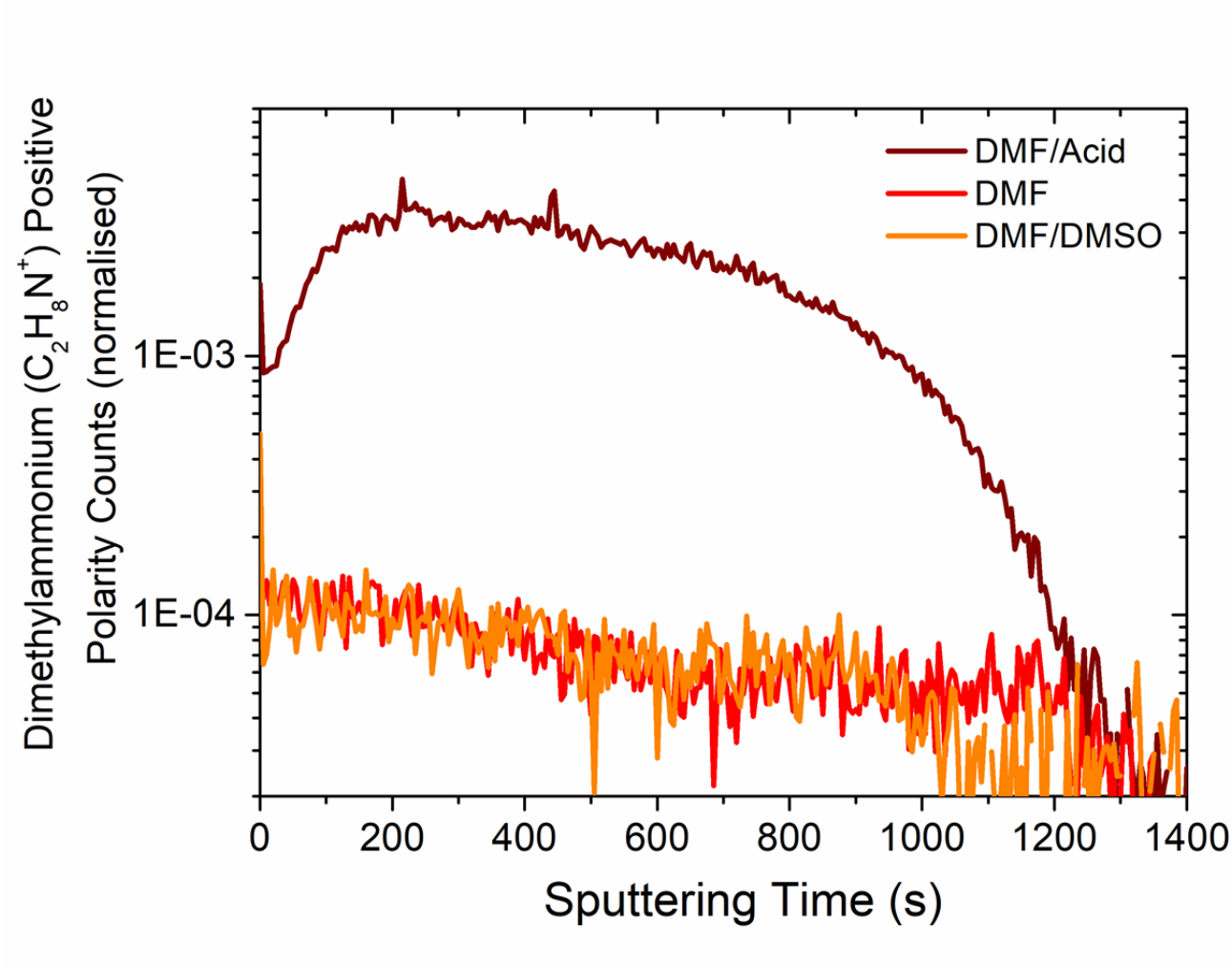


***Figure S1: Positive Polarity Time-of-flight secondary ion mass spectrometry (TOF-SIMS) detecting dimethylammonium $C_2H_8N^+$ ions*** *of (FA, Cs)Pb(Br, I)$_3$ films prepared using various fabrication methods after a 185 °C 90m annealing step.*

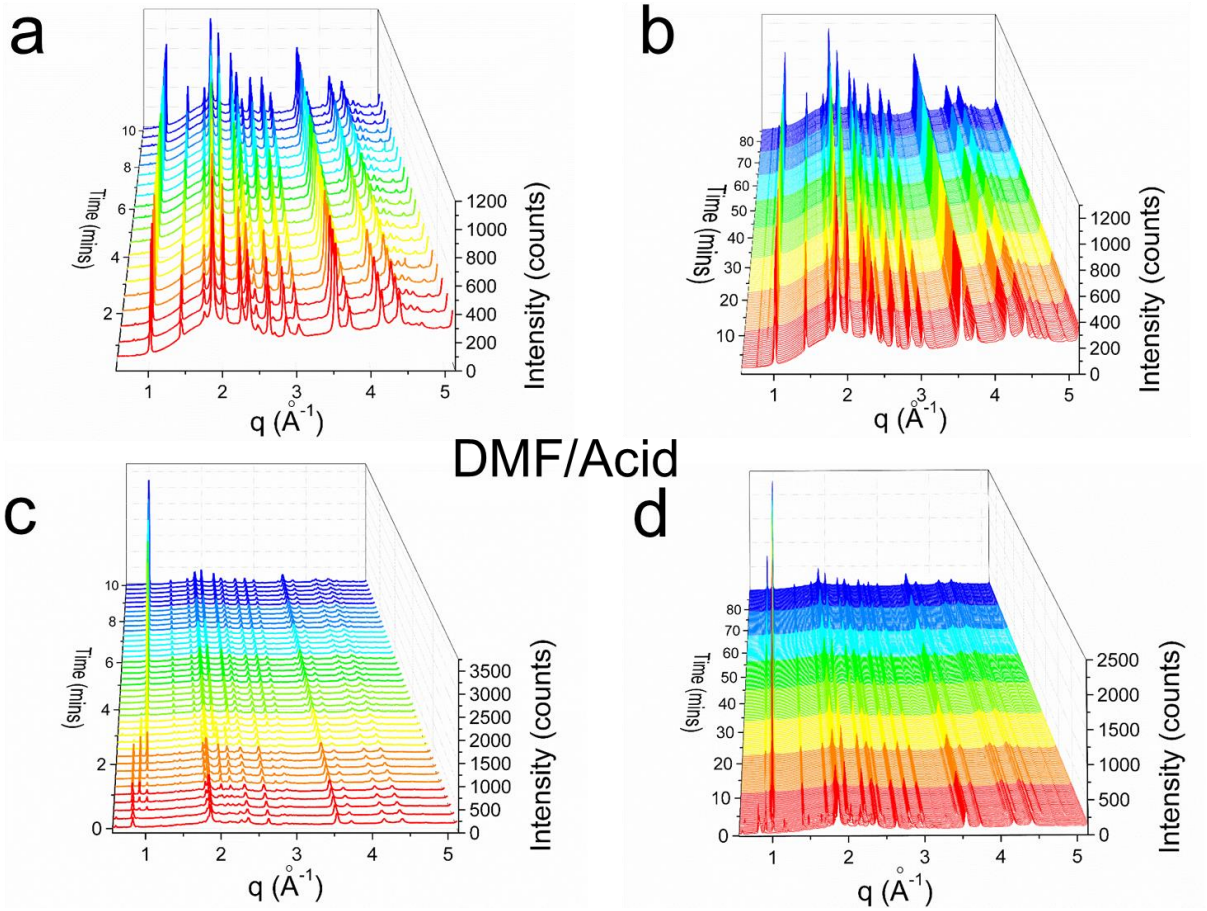


***Figure S2: In-situ crystallization of $FA_{0.83}Cs_{0.17}Pb(I_{0.6}Br_{0.4})_3$ perovskite films comparing a low-temperature DMF/DMSO fabrication method to a high-temperature DMF/Acid fabrication method.*** *Wide-angle X-ray scattering (WAXS) data of a $FA_{0.83}Cs_{0.17}Pb(I_{0.6}Br_{0.4})_3$ perovskite film fabricated with the DMF/DMSO and the DMF/Acid preparation method. The data shows* ***a)*** *the first 10 minutes and* ***b)*** *90 minutes of annealing at 100 ° C. Wide-angle X-ray scattering (WAXS) data of a $FA_{0.83}Cs_{0.17}Pb(I_{0.6}Br_{0.4})_3$ perovskite film fabricated with the DMF/Acid method prepared with a "fully-aged" solution, which was aged for more than 72h after the addition of the HI/HBr additive. The data shows* ***c)*** *the first 10 minutes and* ***d)*** *90 minutes of annealing at 185 °C. Annealing was done in a helium atmosphere with slight water/oxygen contamination.*

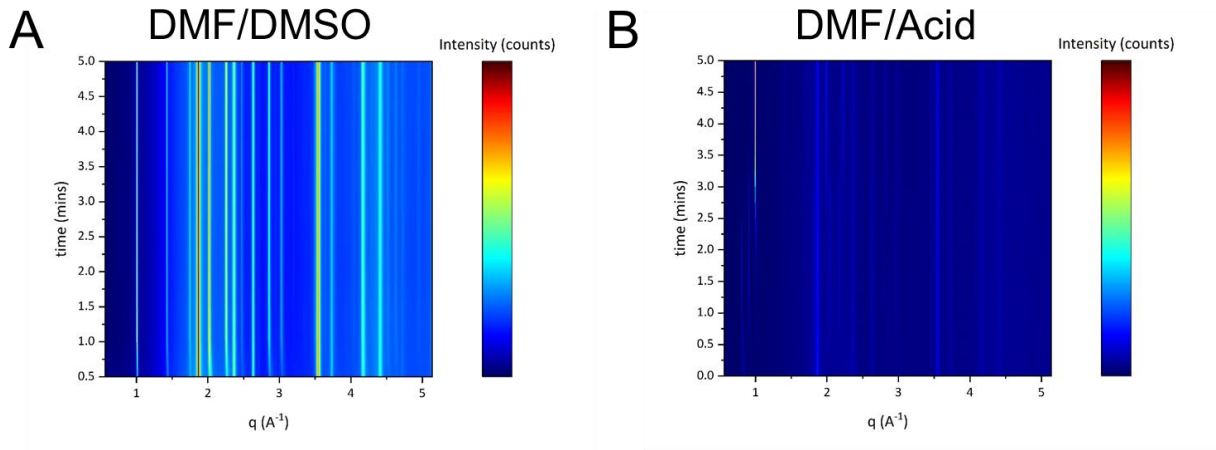


***Figure S3: Wide-angle X-ray scattering (WAXS) 2D waterfall data of a $FA_{0.83}Cs_{0.17}Pb(I_{0.6}Br_{0.4})_3$ perovskite film fabricated with a low-temperature DMF/DMSO and a high-temperature DMF/Acid fabrication method.*** *The data shows the first 5 minutes of a $FA_{0.83}Cs_{0.17}Pb(I_{0.6}Br_{0.4})_3$ perovskite film fabricated with the* ***a)*** *DMF/DMSO fabrication method annealed at 100 °C* ***b)*** *DMF/Acid fabrication method annealed at 185 °C. The DMF/Acid method was prepared with a "fully-aged" solution, which was aged for more than 72h after the addition of the HI/HBr additive. Annealing was done in a helium atmosphere with slight water/oxygen contamination.*

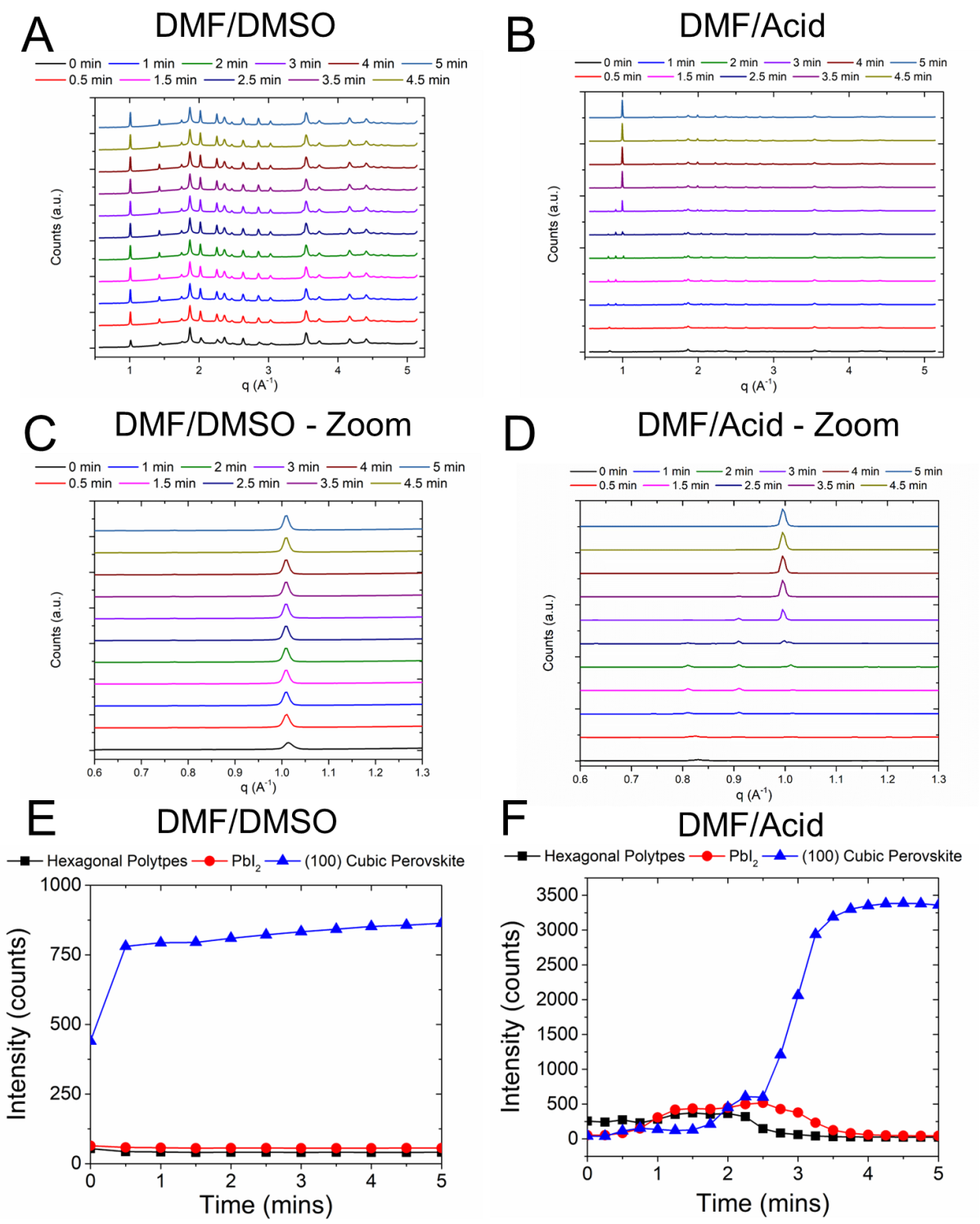


***Figure S4: Wide-angle X-ray scattering (WAXS) 2D layered data and time-traces of individual diffraction peak of a $FA_{0.83}Cs_{0.17}Pb(I_{0.6}Br_{0.4})_3$ perovskite film fabricated with a low-temperature DMF/DMSO and a high-temperature DMF/Acid fabrication method.*** *The data shows the first 5 minutes of a $FA_{0.83}Cs_{0.17}Pb(I_{0.6}Br_{0.4})_3$ perovskite film fabricated with the* ***A, C, E)*** *DMF/DMSO fabrication method annealed at 100 °C* ***B, E, F)*** *DMF/Acid fabrication method annealed at 185 °C. The DMF/Acid method was prepared with a "fully-aged" solution, which was aged for more than 72h after the addition of the HI/HBr additive. Annealing was done in a helium atmosphere with slight water/oxygen contamination.*

We note that the DMF/acid route resulted in a ~50 meV decrease in the bandgap of the pristine film in comparison to the DMF/DMSO route, possibly due to a halide exchange occurring during the crystallization process due to the hydrohalic acids. However, we note that Urbach energy stability improvement cannot simply be attributed to a narrower effective bandgap since the minority phase bandgap for the DMF/DMSO film stabilizes to 1.57 eV, which is 140 meV lower than the stabilized $E_{g,minority}$ for the DMF/acid film. Furthermore, as shown on Fig. S6, for an identical 1.71 eV band gap, the DMF/DMSO $FA_{0.83}Cs_{0.17}Pb(Br_{0.32}I_{0.64})_3$ perovskite film formed a minority phase narrow band gap material significantly faster than a 1.71 eV DMF/DMACl $DMA_{0.3}FA_{0.83}Cs_{0.17}Pb(Br_{0.32}I_{0.64})_3Cl_{0.3}$ perovskite film.

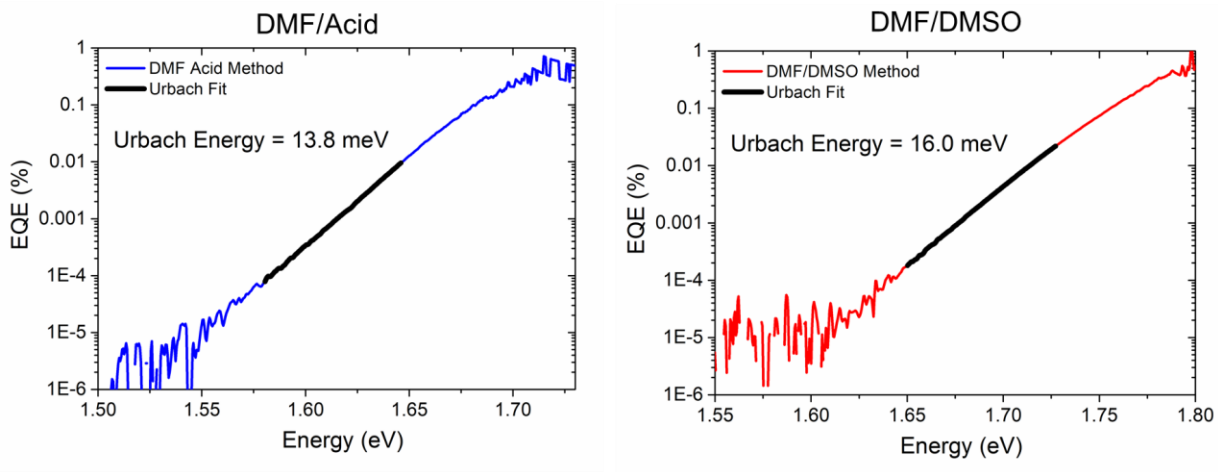


***Figure S5: Semi-log plot of external quantum efficiency (EQE) at the absorption onset*** *of A) a "DMF/Acid" film and B) "DMF/DMSO" film, measured using Fourier-transform photocurrent spectroscopy (FTPS) in short-circuit configuration.*

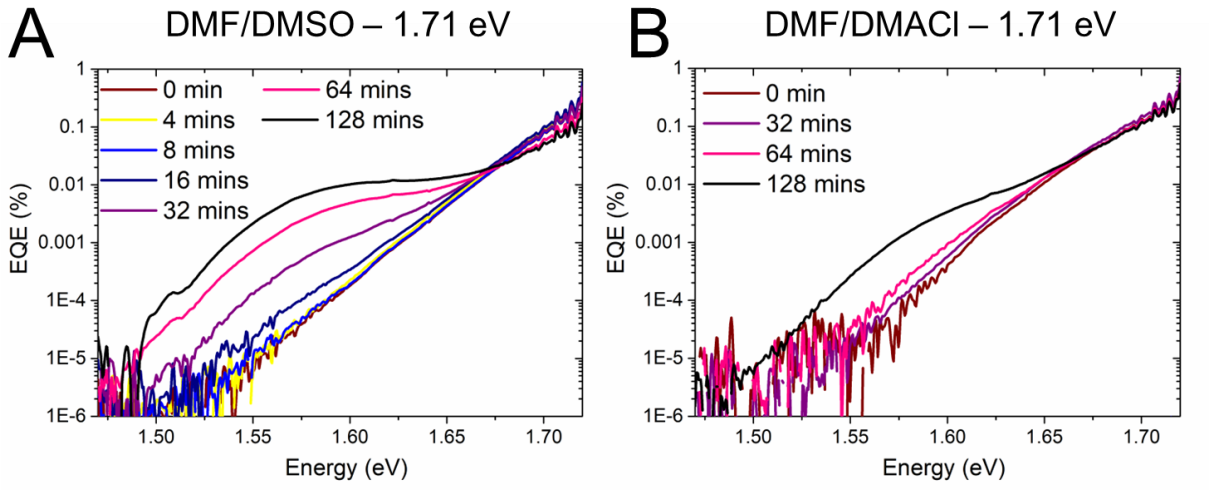


***Figure S6****: External quantum efficiency (EQE), measured via Fourier transform photocurrent spectroscopy for a solar cell with* ***a)*** *a 1.71 eV DMF/DMSO* $FA_{0.83}Cs_{0.17}Pb(Br_{0.32}I_{0.64})_3$ *perovskite film, and with* ***b)*** *a DMF/DMACl* $DMA_{0.3}FA_{0.83}Cs_{0.17}Pb(Br_{0.28}I_{0.72})_3Cl_{0.3}$ *perovskite film. For the EQE measurements, the devices were non-encapsulated and illuminated by a xenon-lamp simulated full-spectrum AM 1.5G, 42 mW cm$^{-2}$ irradiance at open-circuit in air ( ~ 45 RH%) at room temperature.*

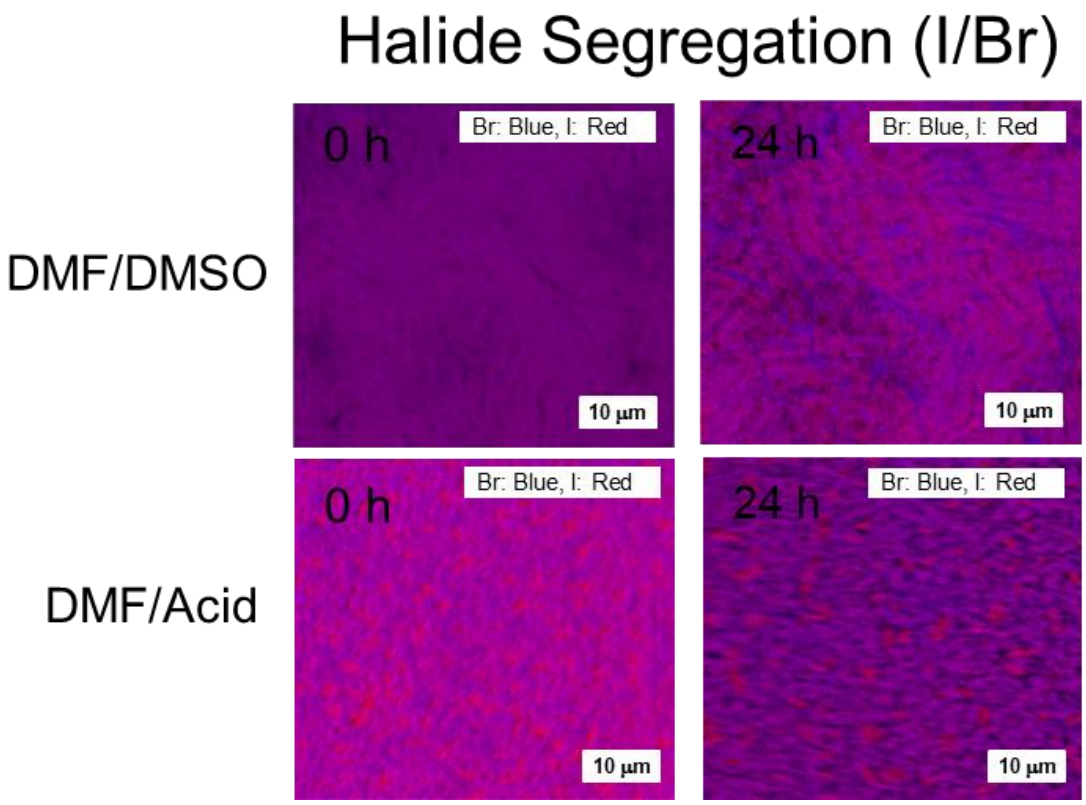


***Figure S7: Formamidinium/caesium A-site cation segregation****. TOF-SIMS 2D mapping of Br (blue) and I (red) overlays for the (**a**) DMF/DMSO, (**b**) DMF/acid devices aged for 0 hours, and **c)** DMF/DMSO **d)** DMF/acid devices aged for 24 hours. The devices were then aged under AM 1.5G sunlight at maximum power point (MPP) in ambient air for 24 hours without encapsulation. All devices were fabricated with a FTO/$SnO_2$/$PC_{61}BM$/$FA_{0.83}Cs_{0.17}Pb(I_{0.6}Br_{0.4})_3$/spiro-OMeTAD/Au architecture. The data was reconstructed to include data only from the perovskite absorber layer from a 3-D tomography dataset of the entire device stack. The images are based on a relative intensity scale for each species, which is shown for each individual image in **Fig. S8**.*

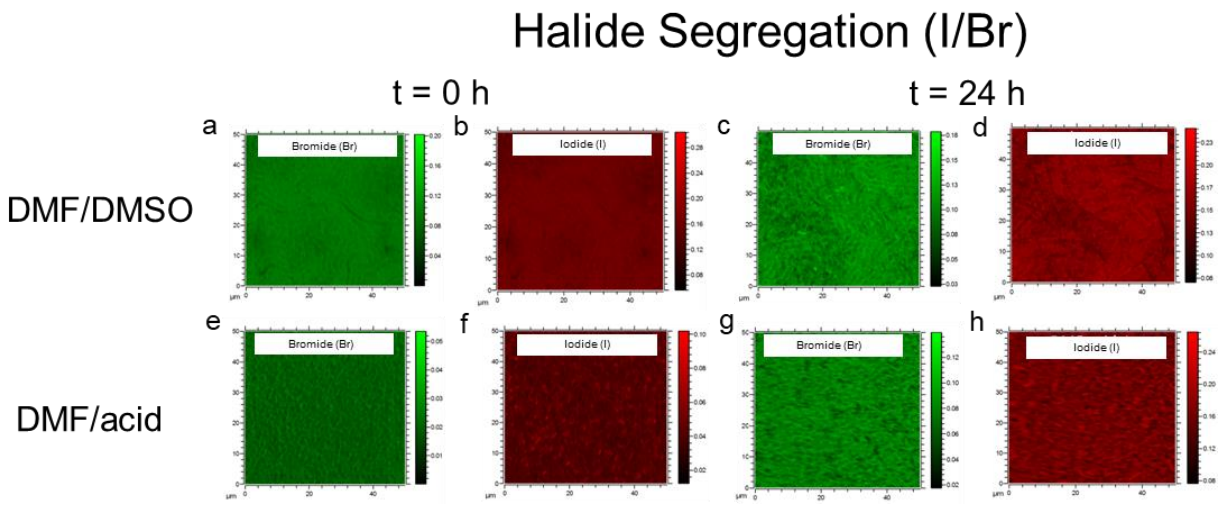


***Figure S8:*** *Light stability of individual halides measured using TOF-SIMS mapping. TOF-SIMS 2D mapping of* ***a)*** *Br and* ***b)*** *I for the DMF/DMSO devices at t = 0 h. TOF-SIMS 2D mapping of* ***c)*** *Br and* ***d)*** *I for the DMF/DMSO devices at t = 24 h. TOF-SIMS 2D mapping of* ***e)*** *Br and* ***f)*** *I for the DMF/acid devices at t = 0 h. TOF-SIMS 2D mapping of* ***g)*** *Br and* ***h)*** *I for the DMF/acid devices at t = 24 h. The devices were aged under AM 1.5G sunlight at maximum power point (MPP) in ambient air for 24 hours without encapsulation. All devices were fabricated with a n-i-p FTO/$SnO_2$/$PC_{61}BM$/$FA_{0.83}Cs_{0.17}Pb(I_{0.6}Br_{0.4})_3$/spiro-OMeTAD/Au architecture. The data was reconstructed to include data only from the perovskite absorber layer from a 3-D tomography dataset of the entire device stack. All the image sizes are 50µm × 50µm. The data were normalized to the total intensity measured at every pixel to minimize topographic effects on the image. Thus the scale at the right of each image is the normalized intensity ($I_{(pixel\ x)}$ /$I_{total\ at\ pixel\ x)}$).*

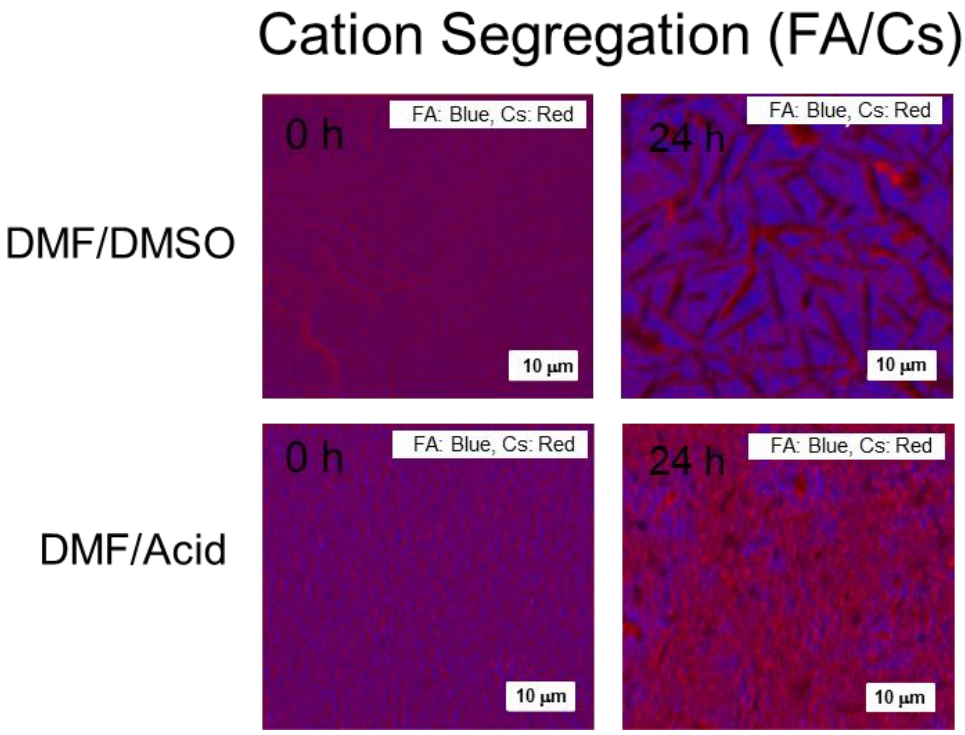


***Figure S9:*** *Formamidinium/caesium A-site cation segregation. TOF-SIMS 2D mapping of FA (blue) and Cs (red) overlays for the (**a**) DMF/DMSO, (**b**) DMF/acid devices aged for 0 hours, and **c)** DMF/DMSO **d)** DMF/acid devices aged for 24 hours. The devices were aged under AM 1.5G sunlight at maximum power point (MPP) in ambient air for 24 hours without encapsulation. All devices were fabricated with a n-i-p FTO/$SnO_2$/$PC_{61}BM$/$FA_{0.83}Cs_{0.17}Pb(I_{0.6}Br_{0.4})_3$/spiro-OMeTAD/Au architecture. The data was reconstructed to include data only from the perovskite absorber layer from a 3-D tomography dataset of the entire device stack. The images are based on a relative intensity scale for each species, which is shown for each individual image in **Fig. S10**.*

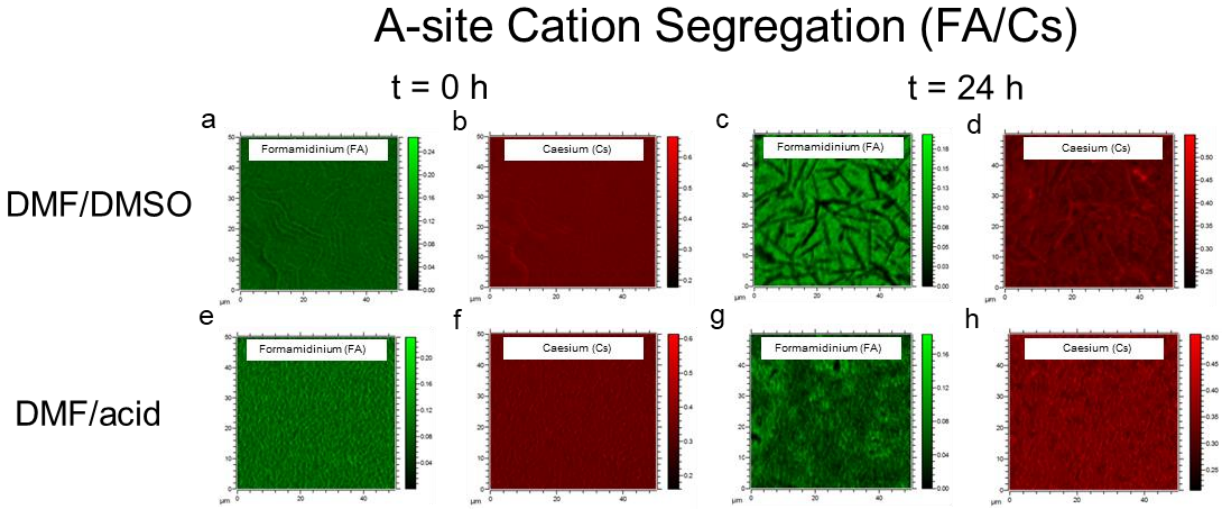


***Figure S10:*** *Light stability of individual A-site cation measured using TOF-SIMS mapping. TOF-SIMS 2D mapping of **a)** FA and **b)** Cs for the DMF/DMSO devices at t = 0 h. TOF-SIMS 2D mapping of **c)** FA and **d)** Cs for the DMF/DMSO devices at t = 24 h. TOF-SIMS 2D mapping of **e)** FA and **f)** Cs for the DMF/acid devices at t = 0 h. TOF-SIMS 2D mapping of **g)** FA and **h)** Cs for the DMF/acid devices at t = 24 h. The devices were aged under AM 1.5G sunlight at maximum power point (MPP) in ambient air for 24 hours without encapsulation. All devices were fabricated with a n-i-p FTO/$SnO_2$/$PC_{61}BM$/$FA_{0.83}Cs_{0.17}Pb(I_{0.6}Br_{0.4})_3$/spiro-OMeTAD/Au architecture. The data was reconstructed to include data only from the perovskite absorber layer from a 3-D tomography dataset*

*of the entire device stack. All the image sizes are 50 µm × 50 µm. The data were normalized to the total intensity measured at every pixel to minimize topographic effects on the image. Thus the scale at the right of each image is the normalized intensity* ($I_{(pixel\ x)} / I_{total\ at\ pixel\ x)}$).

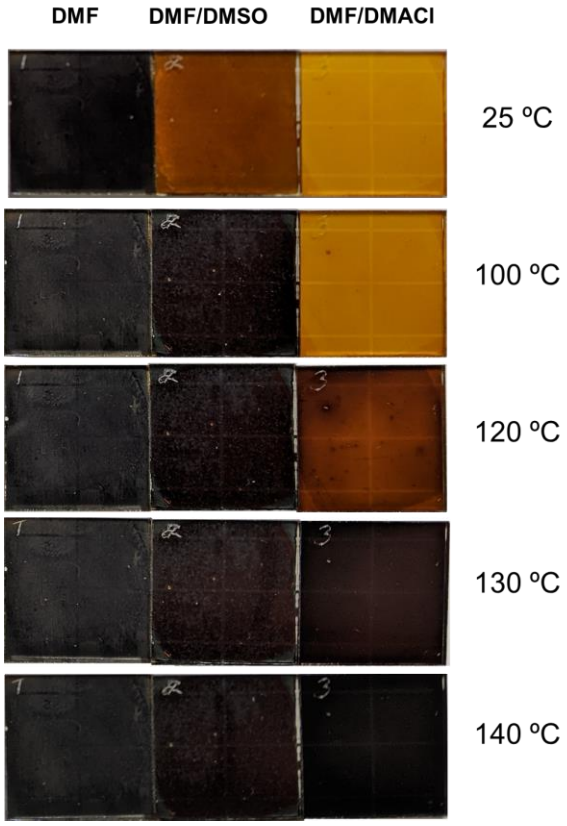


***Figure S11: Impact of temperature on the various film preparation methods DMF, DMF/DMSO and DMF/DMACl. The films were heated at 25 °C, 100 °C, 120 °C, 130 °C and 140 °C for 1 minute in an air atmosphere.*** *The neat DMF film appeared black immediately after spin coating, while the DMF/DMSO and DMF/DMACl had a translucent appearance after spin coating and only at a temperature above 100 °C and 140 °C that these films appeared black. All images were captured on the FTO glass side.*

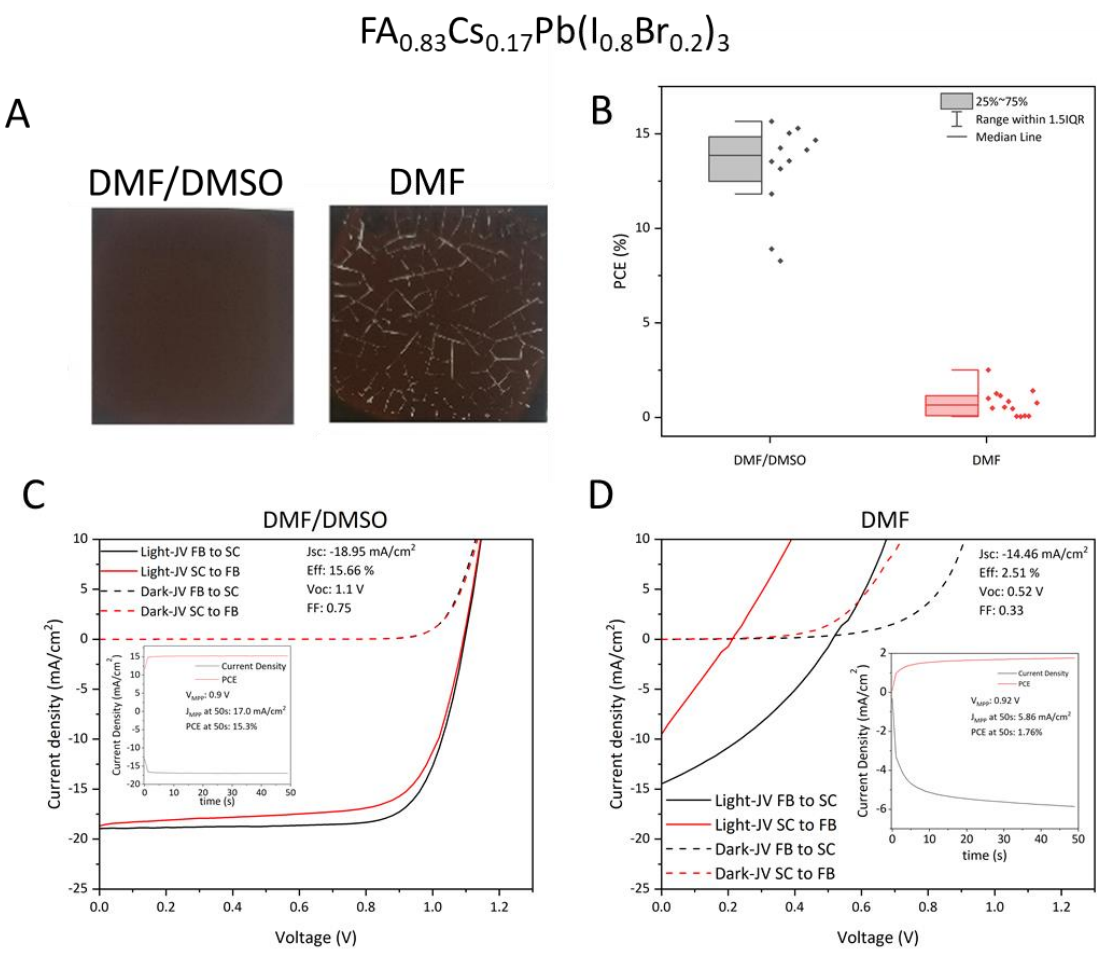


***Figure S12: Comparison between a DMF/DMSO and a neat DMF solvent mixture for perovskite devices.*** *A) ) Images of a backlit perovskite films prepared with a DMF/DMSO and a neat DMF solvent mixture. B) PCE comparison between both methods. C) JV characteristics and stabilized efficiency of a DMF/DMSO device D) JV characteristics of a neat DMF device.*

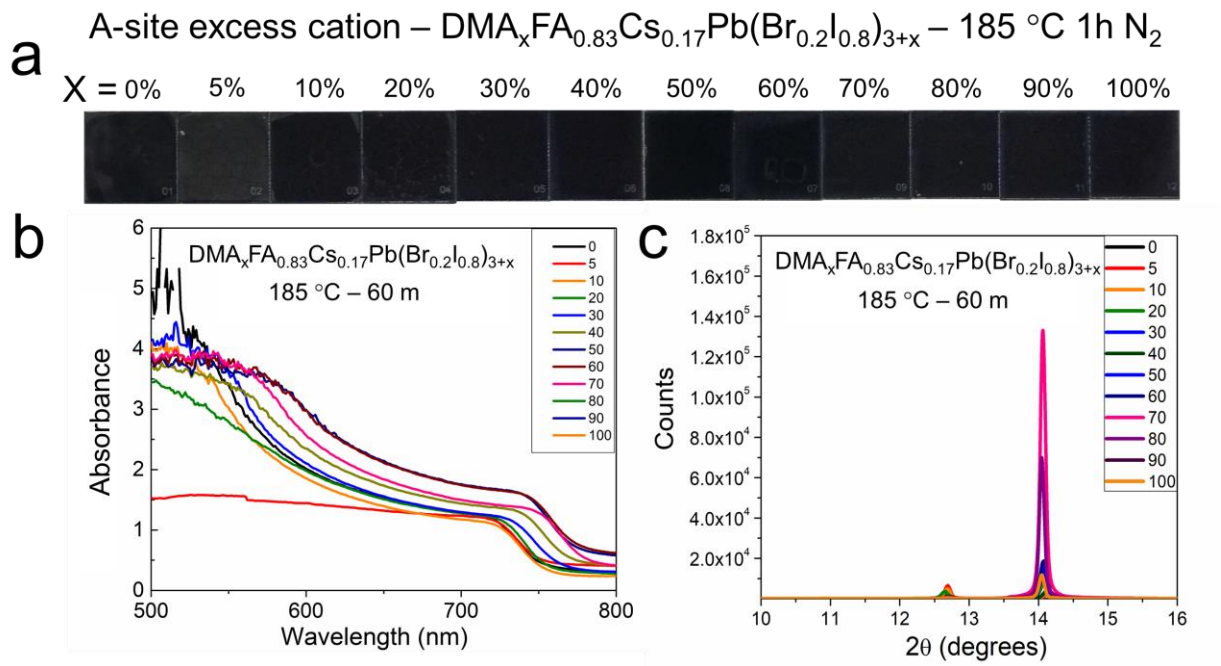


***Figure S13: A-site excess cation of the $DMA_xFA_{0.83}Cs_{0.17}Pb(Br_{0.2}I_{0.8})_{3+x}$ perovskite system after a 60 mins anneal at 185 °C.*** *a) A series of photographs b) X-Ray diffraction patterns c) Ultraviolet-visible (UV-Vis) absorbance spectra of corresponding thin films.*

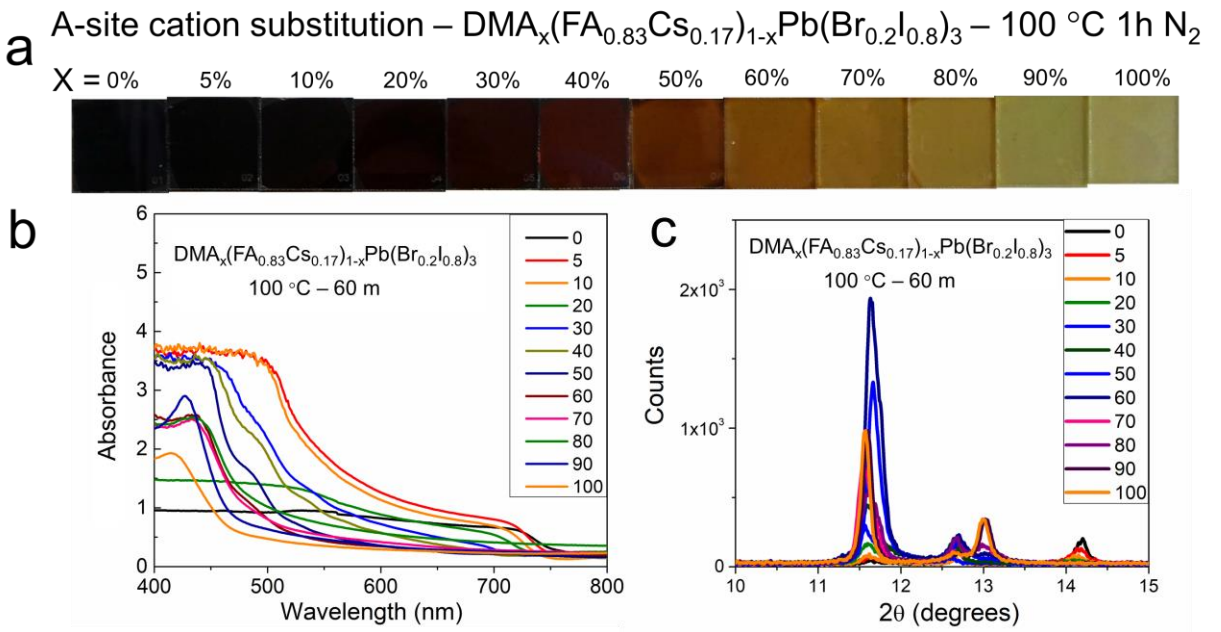


***Figure S14: A-site cation substitution of the $DMA_x(FA_{0.83}Cs_{0.17})_{1-x}Pb(Br_{0.2}I_{0.8})_3$ perovskite system after 60 mins anneal at 100 °C.*** *a) A series of photographs b) X-Ray diffraction patterns c) Ultraviolet-visible (UV-Vis) absorbance spectra of corresponding thin films.*

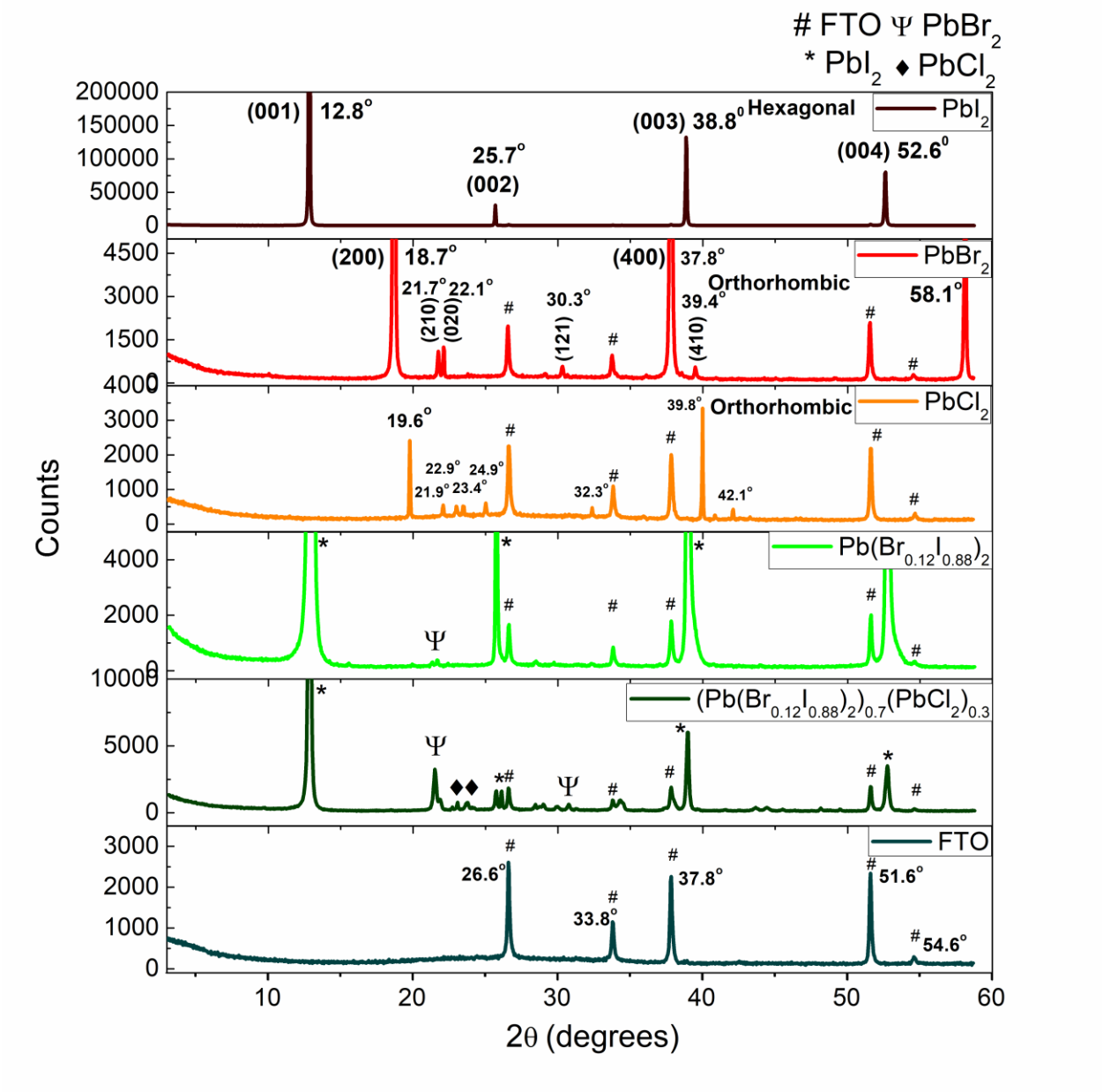


***Figure S15: X-Ray diffraction pattern (XRD) for several $PbX_2$ compositions formed on fluorine-doped tin oxide (FTO) coated glass substrates when annealed at 100 °C for 5 m.***

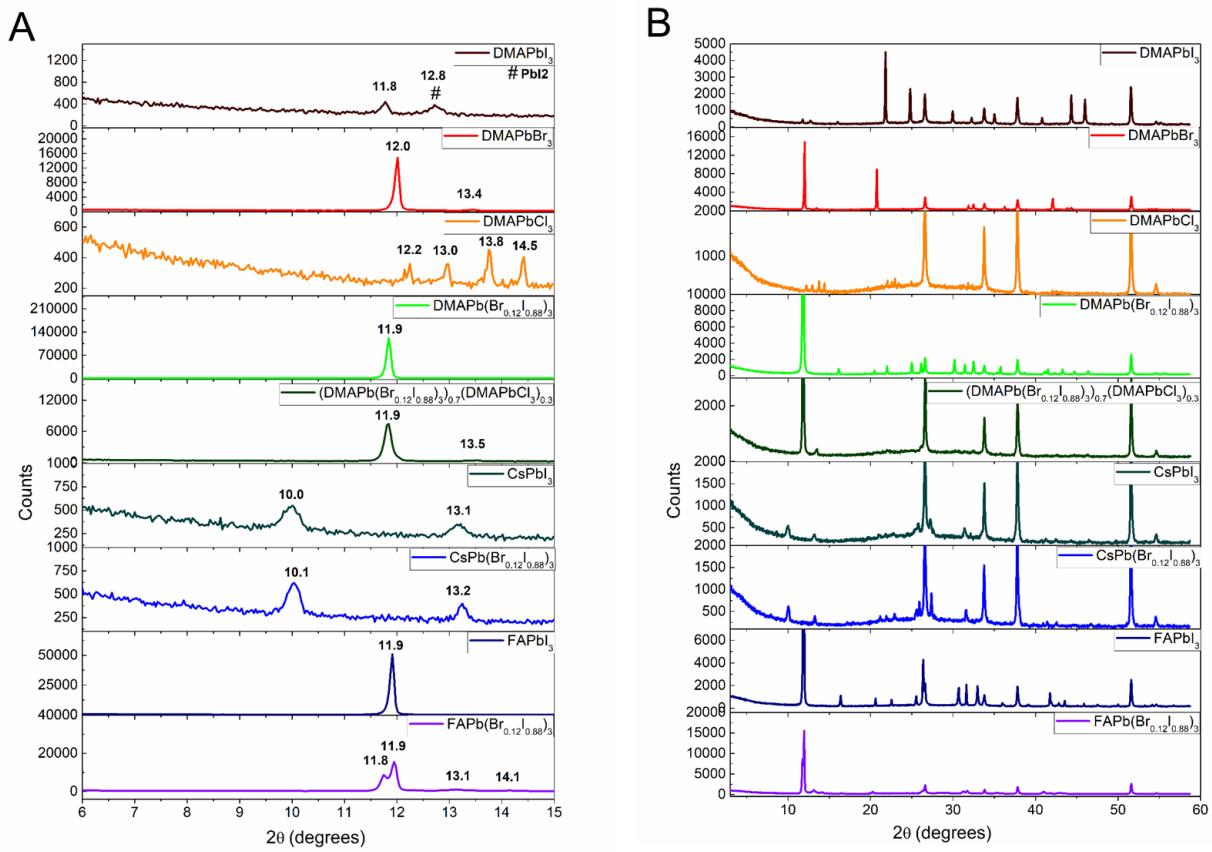


***Figure S16: X-ray diffraction pattern (XRD) for $DMAPbI_3$, $DMAPbBr_3$, $DMAPbCl_3$, $DMAPb(Br_{0.12}I_{0.88})_3$, $(DMAPb(Br_{0.12}I_{0.88})_3)_{0.7}$ $DMAPbCl_3)_{0.3}$, $CsPbI_3$, $CsPb(Br_{0.12}I_{0.88})_3$, $FAPbI_3$, $FAPb(Br_{0.12}I_{0.88})_3$ compositions formed on fluorine-doped tin oxide (FTO) coated glass substrates when annealed at 100 °C for 5 m. We show the XRD for these perovskite compounds from A) $2\theta$ 6 to 15° and B) $2\theta$ 3 to 60°.***

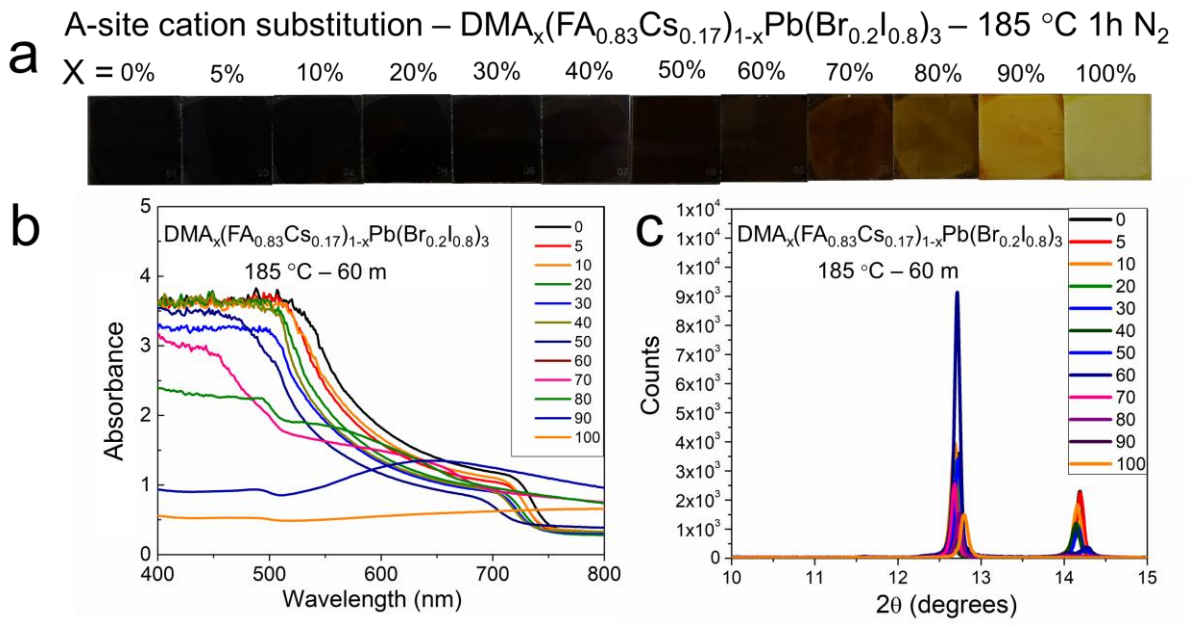


***Figure S17: A-site cation substitution of the $DMA_x(FA_{0.83}Cs_{0.17})_{1-x}Pb(Br_{0.2}I_{0.8})_3$ perovskite system after a 60 m anneal at 185 °C.*** *A) A series of photographs B) X-Ray diffraction patterns C) Ultraviolet-visible (UV-Vis) absorbance spectra of corresponding thin films.*

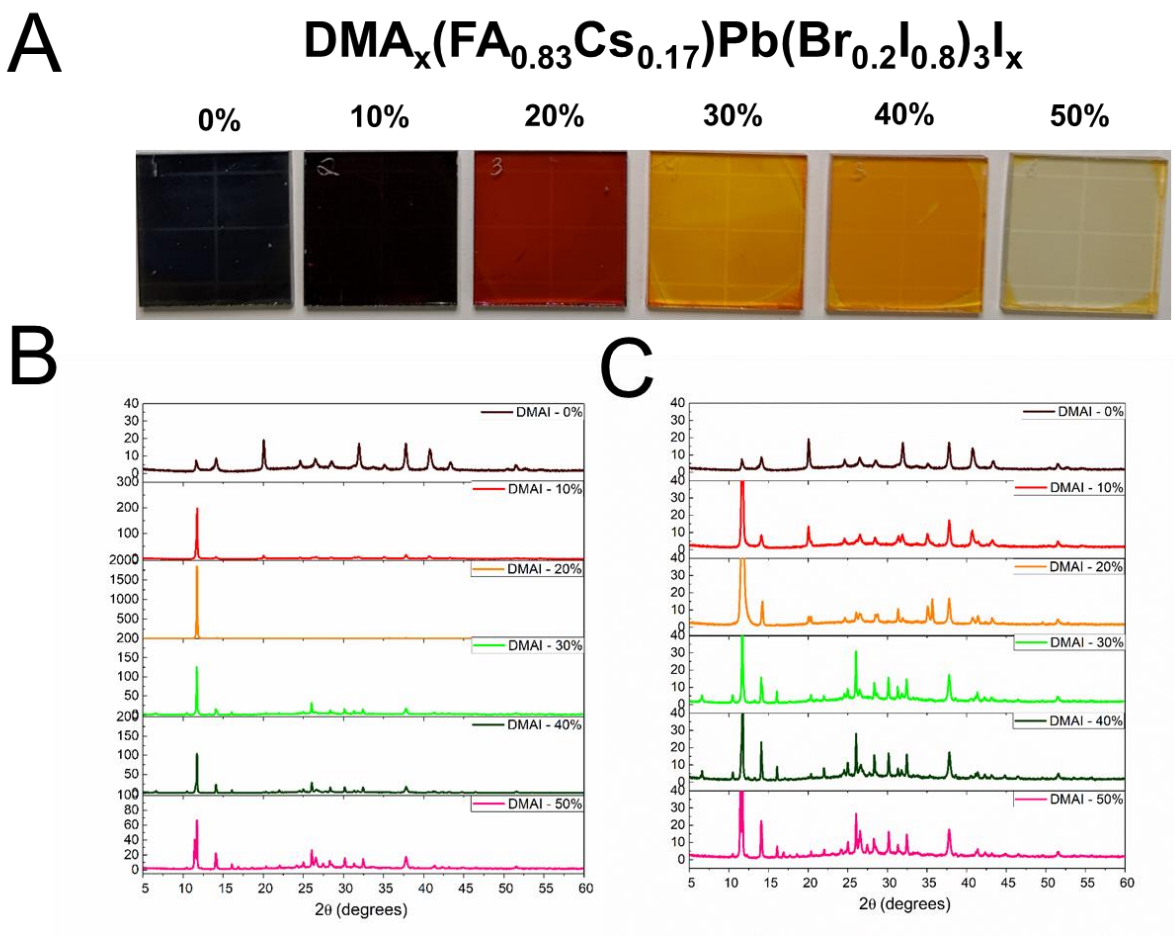


***Figure S18: Impact of DMAI on the intermediate phases of the $FA_{0.83}Cs_{0.17}Pb(Br_{0.8}I_{0.2})_3$*** *A) A series of photographs of $DMA_xFA_{0.83}Cs_{0.17}Pb(Br_{0.8}I_{0.2})_3I_x$ perovskite films spin-coated heated at 100 °C for 1m, with various amounts of DMAI additive, where percentages are expressed in excess amounts with respect to lead. B) A series of X-Ray diffraction patterns of the corresponding thin film showing the intermediate precursor phases in the form of hexagonal polytypes. C) A series of zoom-in graphs of the corresponding XRD patterns.*

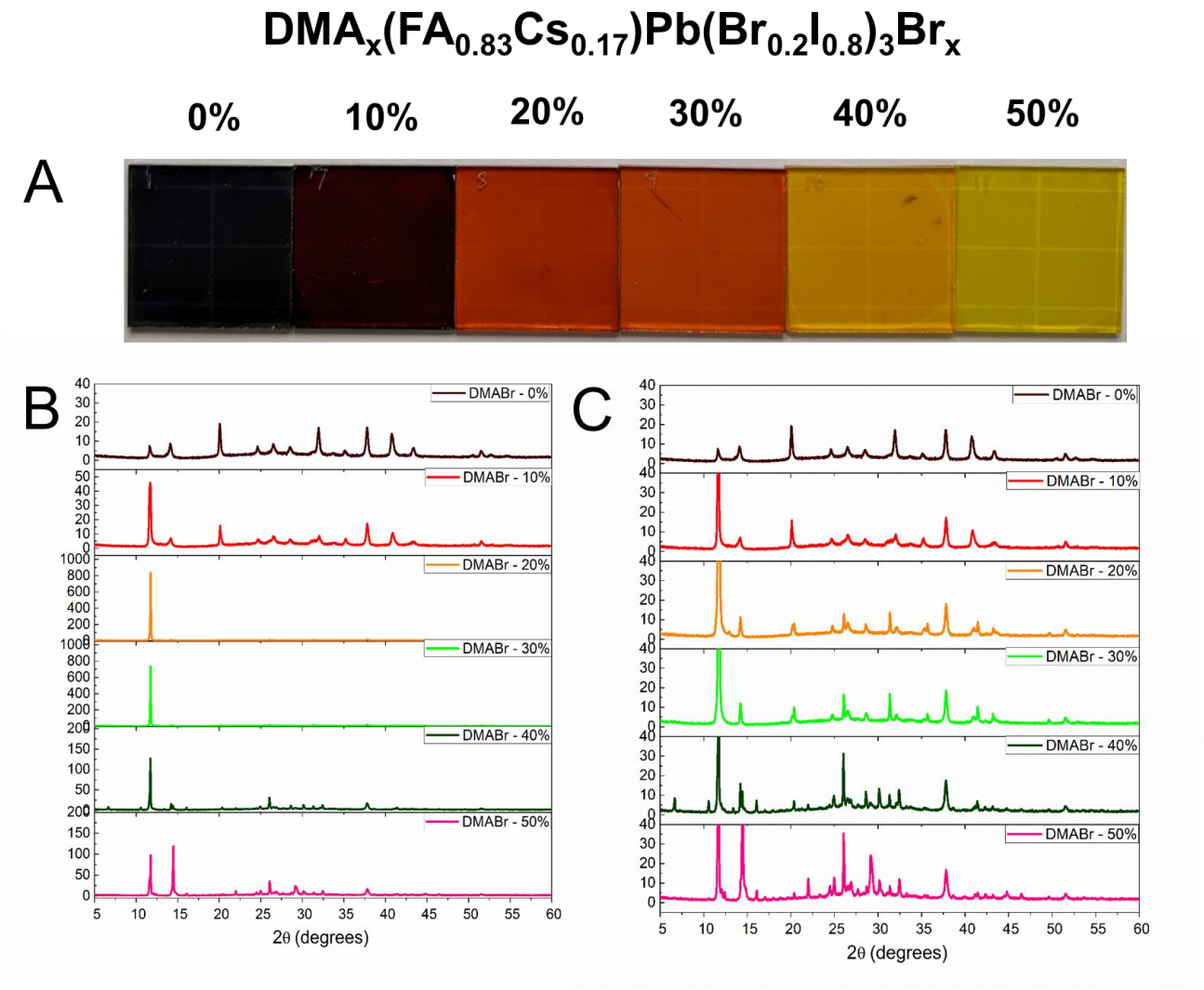


***Figure S19: Impact of DMABr on the intermediate phases of the $FA_{0.83}Cs_{0.17}Pb(Br_{0.8}I_{0.2})_3$.*** *A) A series of photographs of $DMA_xFA_{0.83}Cs_{0.17}Pb(Br_{0.8}I_{0.2})_3I_x$ perovskite films spin-coated heated at 100 °C for 1m, with various amounts of DMABr additive, where percentages are expressed in excess amounts with respect to lead. B) A series of X-Ray diffraction patterns of the corresponding thin film showing the intermediate precursor phases in the form of hexagonal polytypes. C) A series of zoom-in graphs of the corresponding XRD patterns.*

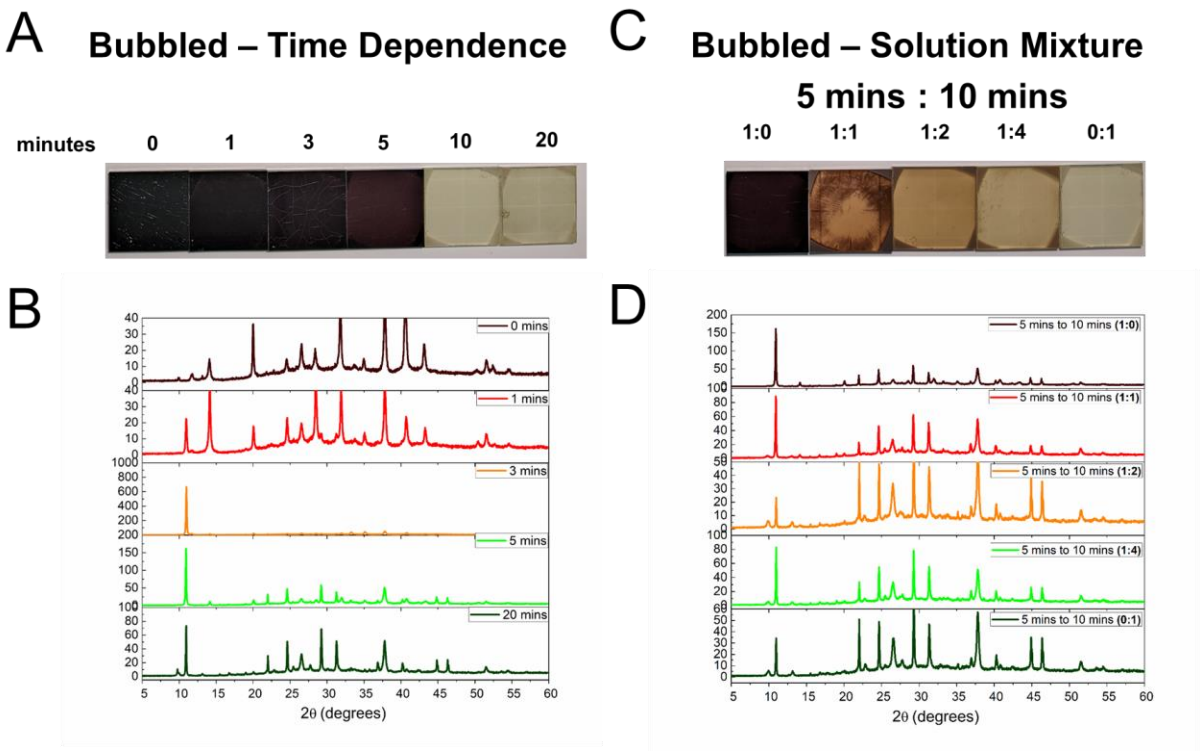


***Figure S20: Impact of bubbling dimethylamine solution into a neat DMF perovskite precursor solution on the intermediate phases of the $FA_{0.83}Cs_{0.17}Pb(Br_{0.8}I_{0.2})_3$.*** *A) A series of photographs of $DMA_xFA_{0.83}Cs_{0.17}Pb(Br_{0.8}I_{0.2})_3$ perovskite films spin-coated heated at 100 °C for 1m, with various amounts of DMA additive, where the amount of DMA is correlated to the amount of time the solution was bubbled for. B) A series of X-Ray diffraction patterns of the corresponding thin film showing the intermediate precursor phases in the form of hexagonal polytypes. C) A series of photographs of $DMA_xFA_{0.83}Cs_{0.17}Pb(Br_{0.8}I_{0.2})_3$ perovskite films spin-coated heated at 100 °C for 1m, prepared with various perovskite precursor solutions composed of a mixture between the 5 minutes and the 10 minutes bubbled solution. D) A series of X-Ray diffraction patterns of the corresponding thin film showing the intermediate precursor phases in the form of hexagonal polytypes.*

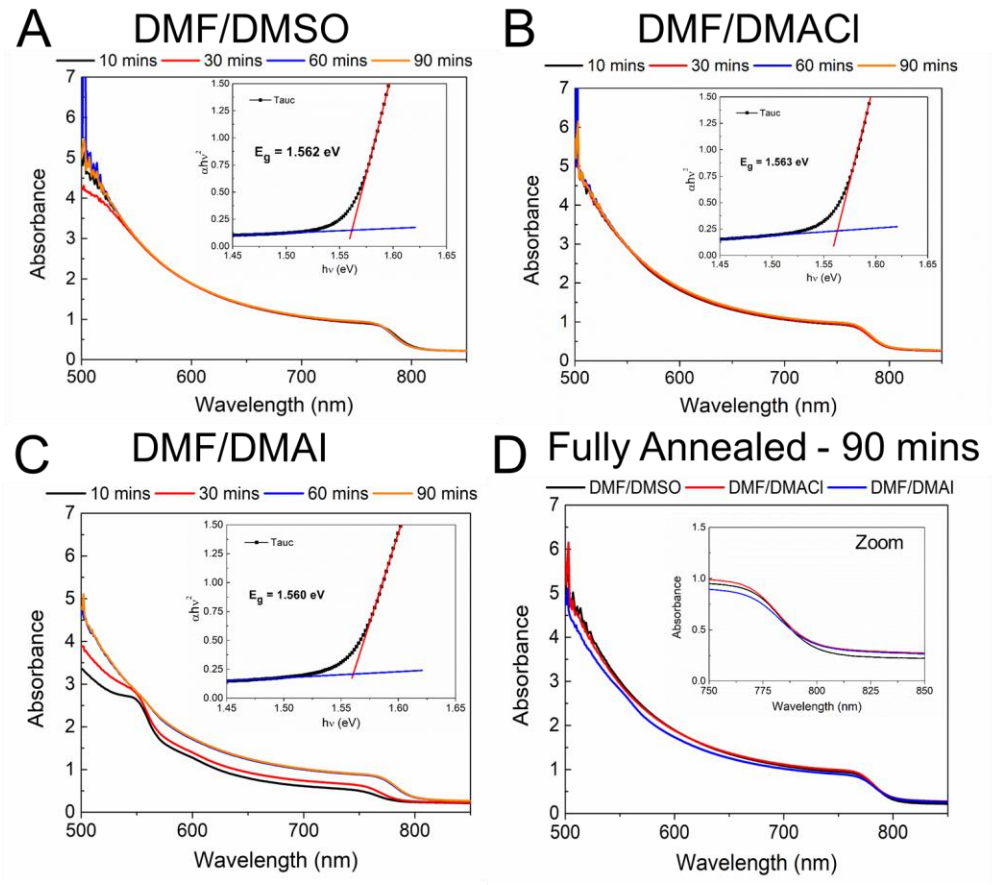


***Figure S21: Optical band gap comparison between the perovskite films prepared with three different precursor solutions: $FA_{0.83}Cs_{0.17}PbI_3$ (DMF/DMSO), $DMA_{0.3}FA_{0.83}Cs_{0.17}PbI_3Cl_{0.3}$ (DMF/DMACl), $DMA_{0.3}FA_{0.83}Cs_{0.17}PbI_{3.3}$ (DMF/DMAI).*** *All films were characterized throughout the annealing process after a 10 mins of annealing at 170 °C on a hotplate, and a subsequent annealing in an oven at 175 °C after 30, 60 and 90 mins. A series of Ultraviolet-visible (UV-Vis) absorbance spectra measured throughout the annealing process of a film prepared with a precursor solution composed of* ***A)*** *$FA_{0.83}Cs_{0.17}PbI_3$ (DMF/DMSO)* ***B)*** *$DMA_{0.3}FA_{0.83}Cs_{0.17}PbI_3Cl_{0.3}$ (DMF/DMACl)* ***C)*** *$DMA_{0.3}FA_{0.83}Cs_{0.17}PbI_{3.3}$ (DMF/DMAI).* ***D)*** *A UV-Vis comparison spectra of a series of fully annealed films.*

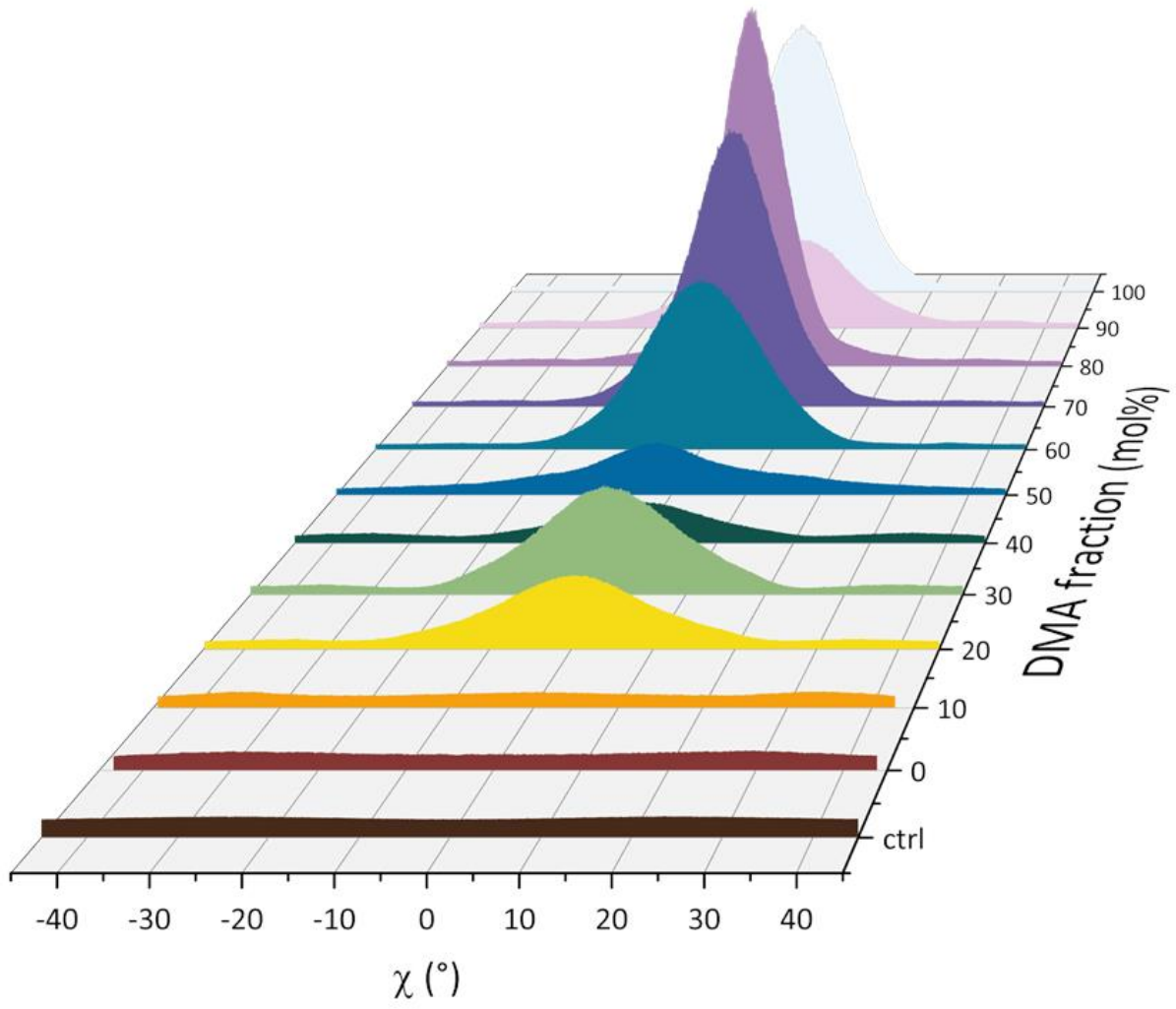


***Figure S22: A 2D XRD beta peak analysis**, showing the (100) peak intensity as a function of the azimuth angle (χ) for a series $DMACl_x(FA_{0.83}Cs_{0.17})Pb(I_{0.8}Br_{0.2})_3$ perovskite film.*

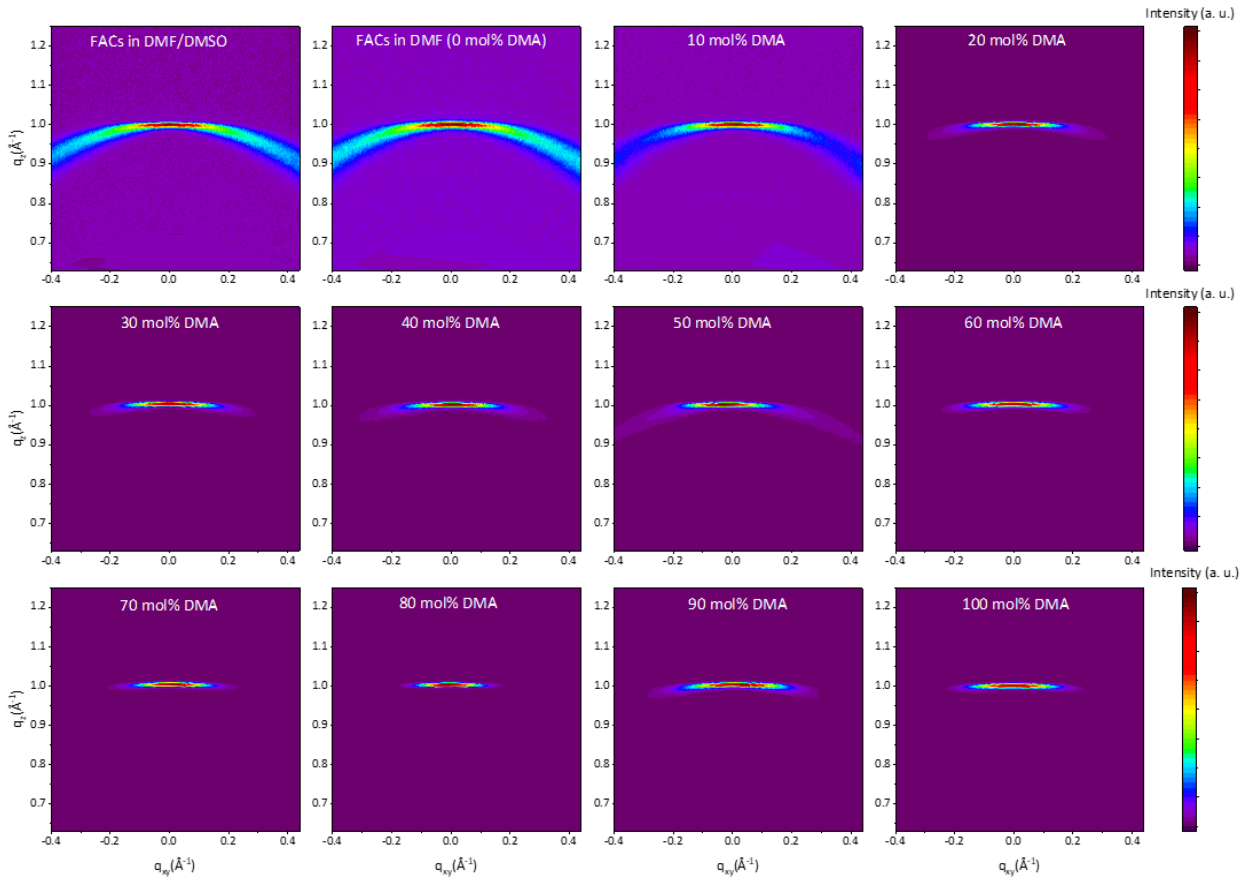


***Figure S23*** **2D XRD of the (100) peak of a $FA_{0.83}Cs_{0.17}Pb(I_{0.85}Br_{0.15})_3$ perovskite film prepared using DMF/DMSO and a series of $DMA_xFA_{0.83}Cs_{0.17}Pb(I_{0.85}Br_{0.15})_3Cl_x$ dissolved DMF only.**

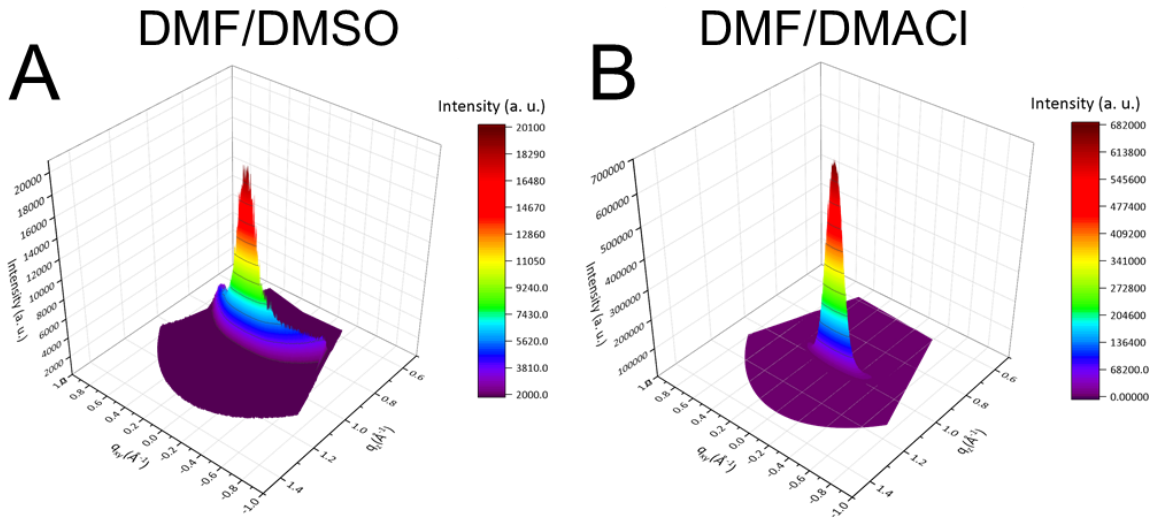


***Figure S24: A 3D dimensional plot of a 2D XRD beta peak analysis, showing the intensity of the (100) peak as a function of $q_y$ and $q_z$ for the* A)** *DMF/DMSO - $FA_{0.83}Cs_{0.17}Pb(I_{0.8}Br_{0.2})_3$ and the* **B)** *DMF/DMACl - $DMA_x(FA_{0.83}Cs_{0.17})Pb(I_{0.8}Br_{0.2})_3Cl_x$ perovskite film.*

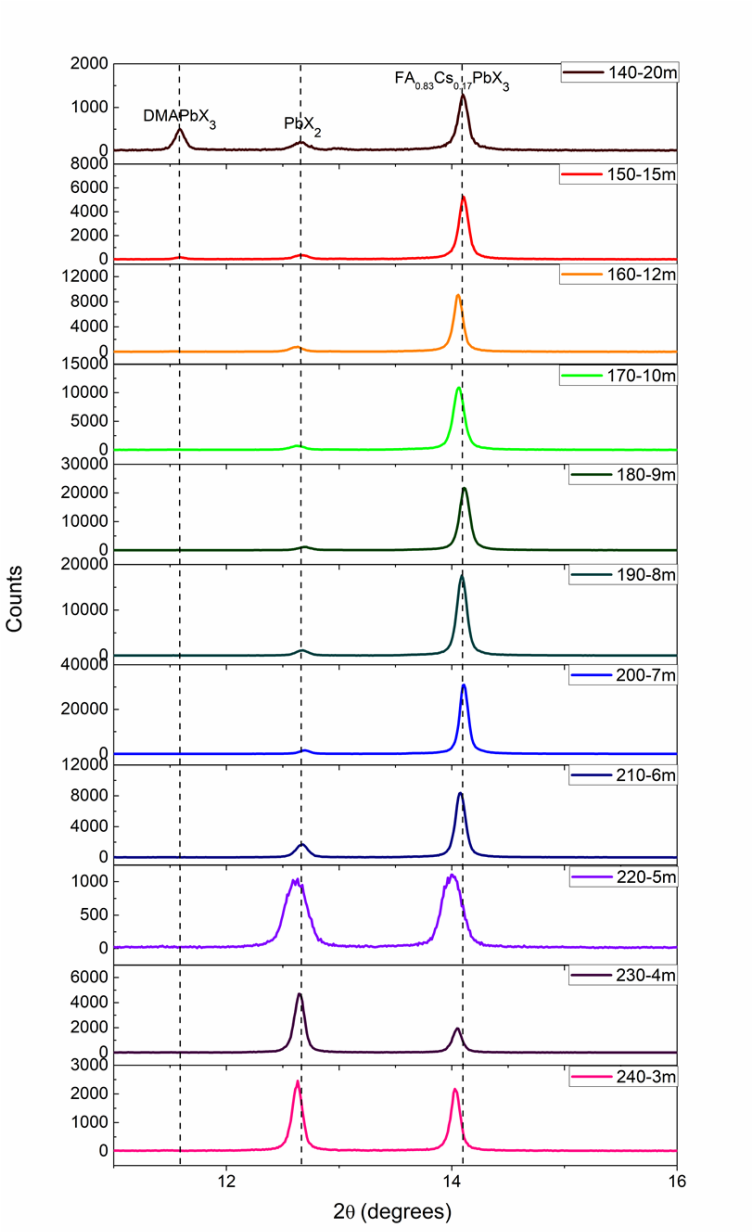


***Figure S25: A series of $DMA_x(FA, Cs)_{1-x}Pb(Br, I)_3Cl_x$ perovskite films after various annealing conditions varying time and temperature.***

We present in **Fig. S26B-D** the UV-Vis absorption spectra, and the XRD pattern zoomed in the 2θ ≈ 10-15° of the corresponding films in **Fig. S26A**. In **Fig. S26B** we observe that the DMF/DMSO perovskite films show a significant shift in the absorption onset to a shorter energy wavelength within the first few hours of heating and a complete loss of the perovskite absorption onset after 24 h of heating. On the other hand, as shown in **Fig. S26C**, the DMF/acid perovskite films show a degradation rate roughly half that of the DMF/DMSO films for $FA_{0.83}Cs_{0.17}Pb(I_{0.6}Br_{0.4})_3$, where we observe a disappearance of their absorption onset after 40 h. We observed a widening of the optical band gap over time and a shift in the 14° XRD perovskite (100) peak to larger 2θ angles. A shift of the (100) peak to larger 2θ angles indicates a contraction of the crystal lattice, caused by a compositional change of the perovskite to a higher bromide to iodide ratio. Hence, we hypothesize that the larger iodide species appear to leave the crystal structure at a faster rate than the smaller bromide halogen. From the XRD, we observe the rise of the $PbX_2$ peak located around 2θ ≈ 12.7°. We plot the variations of the XRD peak intensity ratio of the $PbX_2$ peak to the cubic (100) perovskite peak, where we also identify the slower degradation rate in the DMF/acid films.

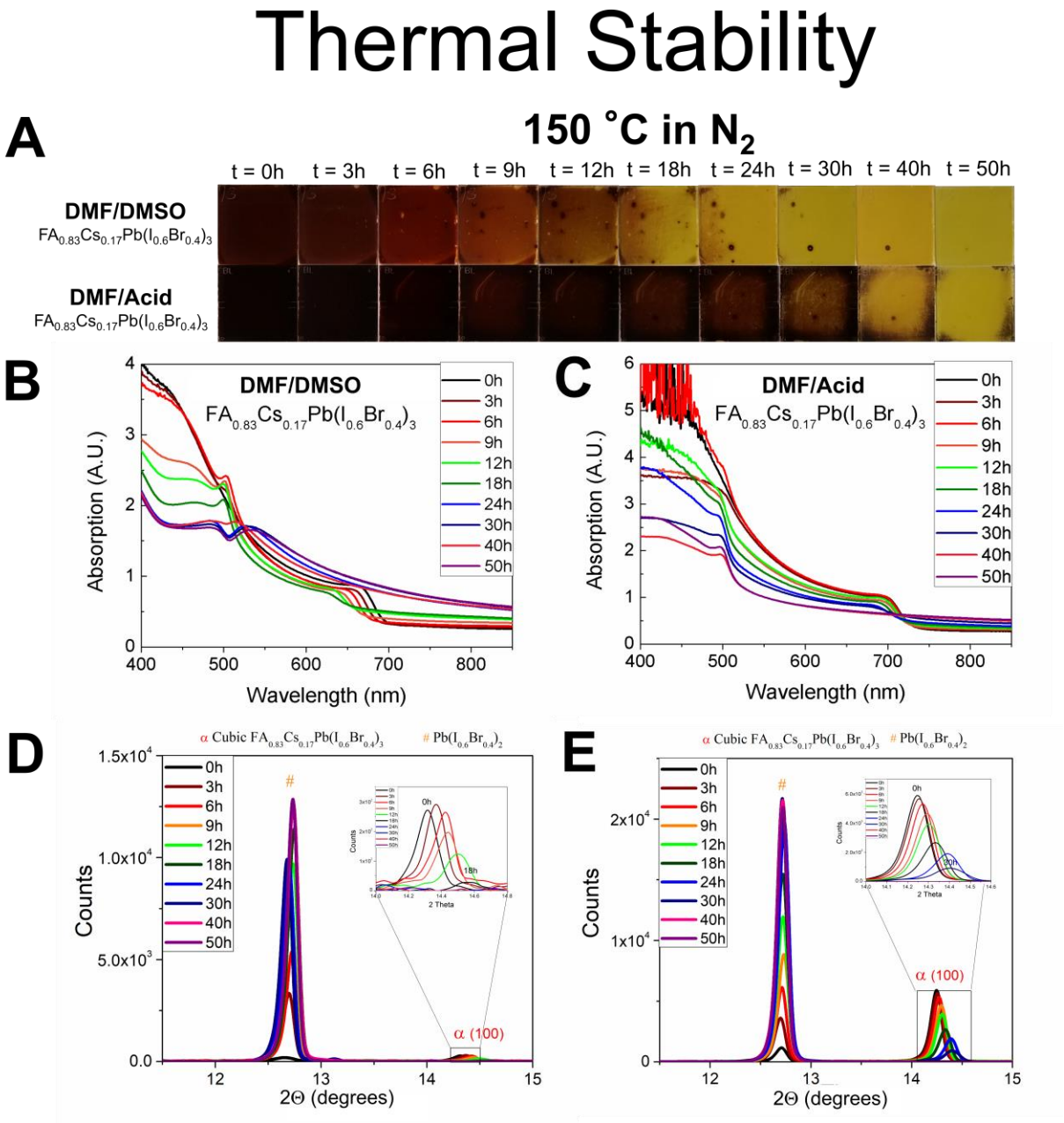


**Figure S26: Thin film thermal stability. A)** Photographs of $FA_{0.83}Cs_{0.17}Pb(I_{0.6}Br_{0.4})_3$ perovskite thin films when heated at 150 °C in a $N_2$ atmosphere. The top row shows films fabricated with the standard DMF/DMSO fabrication method, and the bottom row shows films fabricated with the DMF/Acid fabrication method. **B, C)** UV-Vis absorbance spectra of films of corresponding films. **D, F)** XRD pattern of corresponding films, where # and $\alpha$ stand for the reflections originated from the $PbX_2$ (X is a mixture of I and Br) and cubic $FA_{0.83}Cs_{0.17}Pb(I_{0.8}Br_{0.2})_3$ phase, respectively.

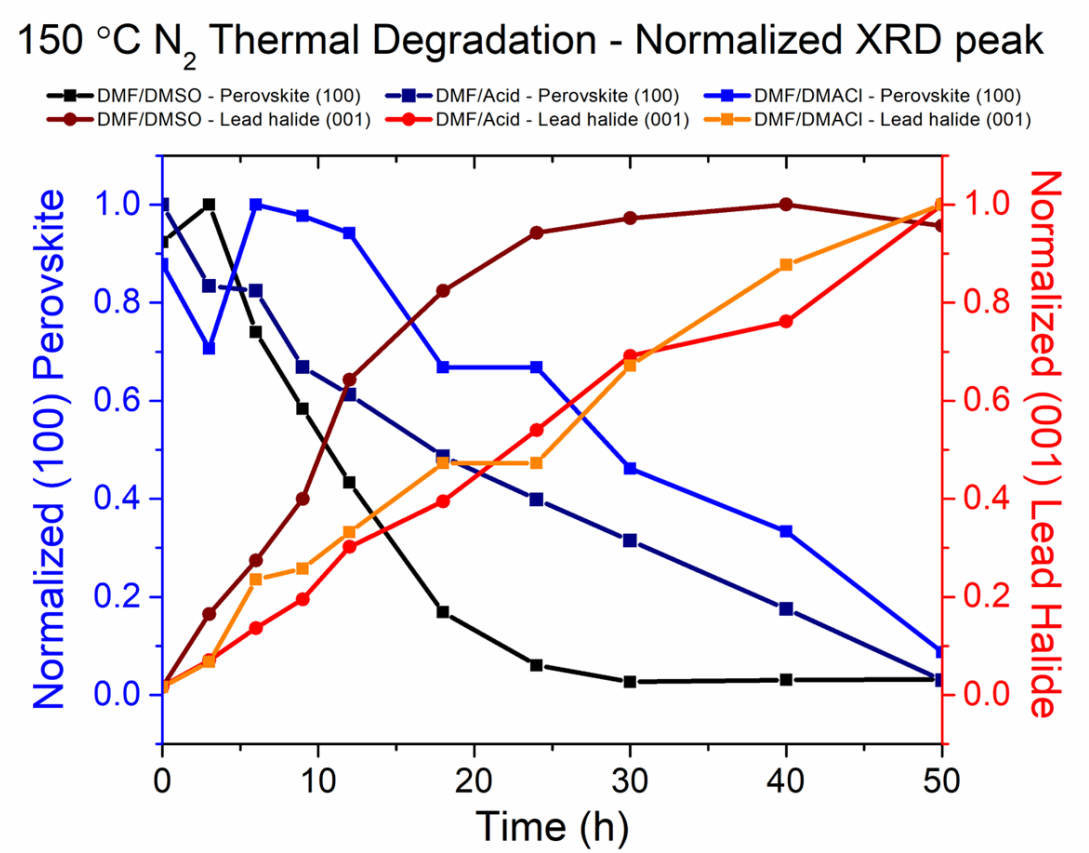


***Figure S27: Evolution of normalised intensity ratio between lead halide and perovskite XRD peak versus thermal aging time.*** *All perovskite films were deposited on a FTO substrate and heated for up to 50 hours on a 150 °C hotplate in a $N_2$-filled glovebox. The three films were prepared with three different preparation methods: DMF/DMSO, DMF/acid, DMF/DMACl. The data for this plot is taken from Fig. 5 of the main manuscript.*

In Fig. S28, we show the TGA weight loss curves along with the 1st derivatives of the TGA heating curves for these different preparation techniques. We observe a 14 °C difference, from 265 to 279 °C, between the peaks of 1st derivative of the highly orientated DMF/DMSO and DMF/acid preparation methods for the narrower bandgap $FA_{0.83}Cs_{0.17}Pb(I_{0.8}Br_{0.2})_3$ perovskite. This difference may appear quite small; however, as shown in Fig. S28, the TGA differential for the 1st derivatives between $MAPbI_3$ and $FAPbI_3$ is 50 °C. Hence, we can expect that a 14 °C represents a significant impact in overall thermal stability, considering that the MA-based perovskite fully degrades within the first hour when heated at 150 °C in a $N_2$ atmosphere (Fig. S29). Therefore, the TGA study shows that the highly textured DMF/acid

method perovskite film exhibits increased thermal stability, beyond the susceptibility to degradation in oxygen and sunlight, in contrast to the isotropic DMF/DMSO perovskite films, which is in good agreement with our thermal stressing results of the thin films.

We note that TGA performed on the thin films shows a significant buoyancy effect[1,2] where the measured mass at an early time exceeds the original mass. This buoyancy phenomenon is caused by the density of the surrounding gas decreasing upon heating, which creates the appearance of the sample gaining weight. The most significant variation in air density occurs at lower temperatures, hence at the beginning of the experiment.

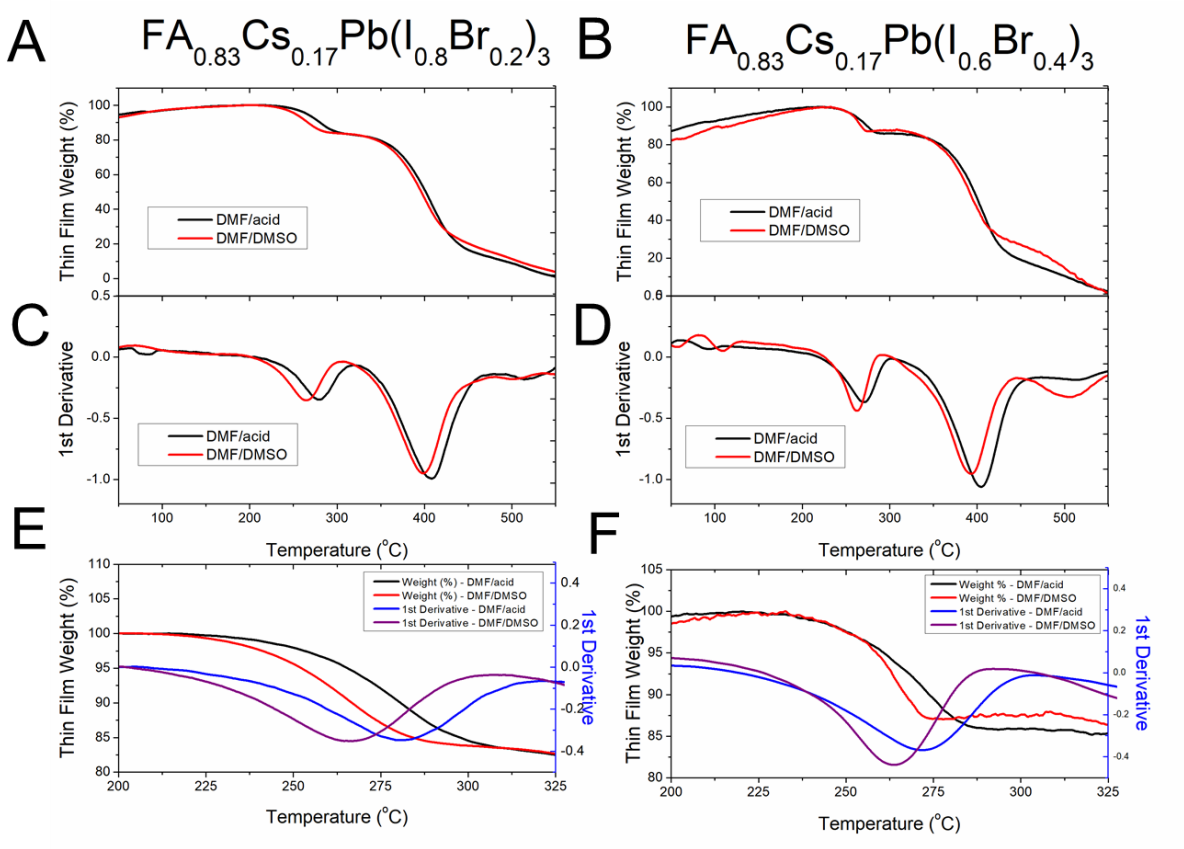


***Figure S28: Thermogravimetric analysis (TGA) of formamidinium-caesium lead mixed-halide perovskite $FA_{0.83}Cs_{0.17}Pb(Br_xI_{(1-x)})_3$ thin films prepared with different preparation techniques.*** *A) TGA heating curves. B) Corresponding first derivatives for the perovskite thin films. C) Magnification showing both heating curve and first derivatives of the temperature region where organic mass loss is prominent.*

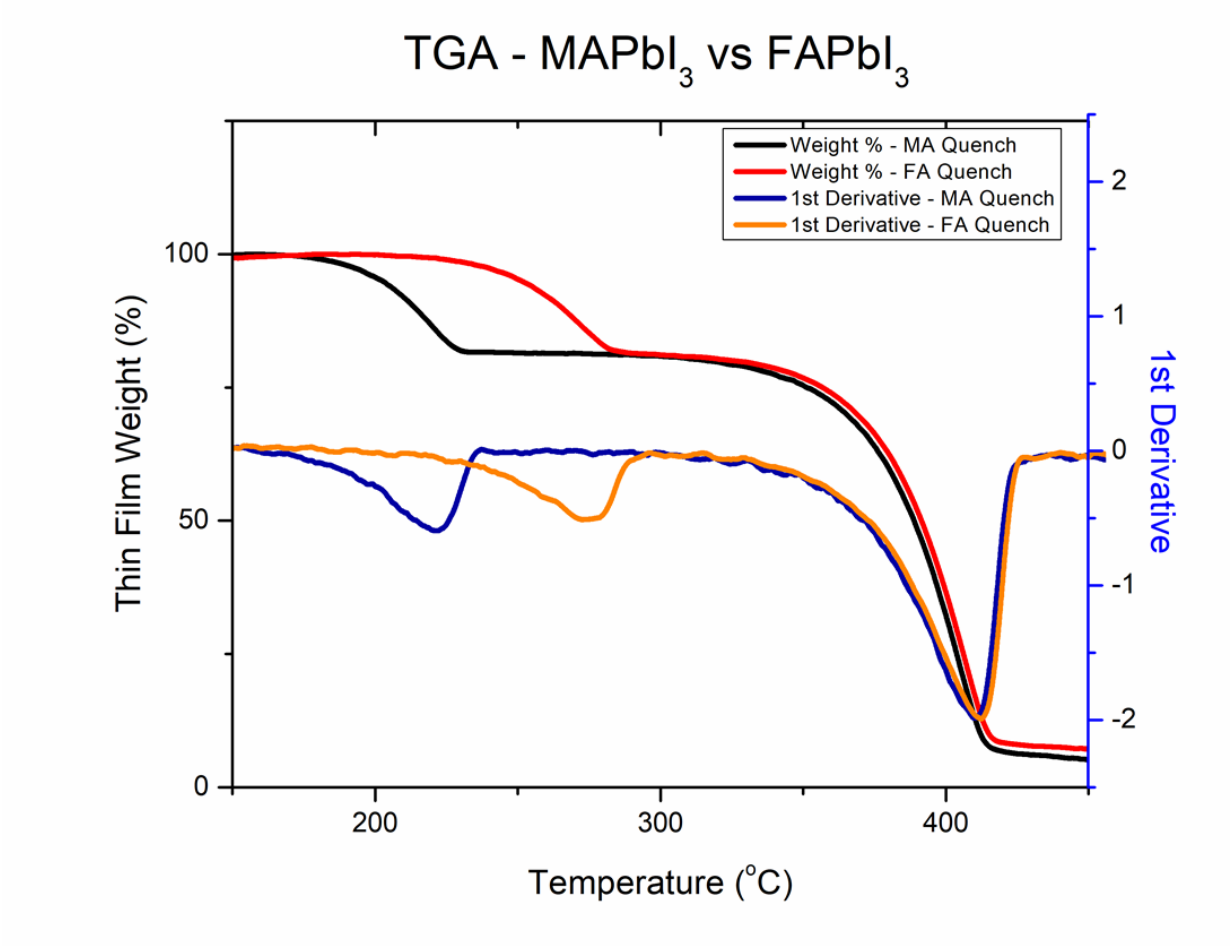


***Figure S29: TGA data of the $MAPbI_3$ compared to the $FAPbI_3$ perovskite films.*** *TGA heating curves and the corresponding first derivative of the $MAPbI_3$ and $FAPbI_3$ perovskite films were prepared using the DMF/DMSO anti-solvent method.*

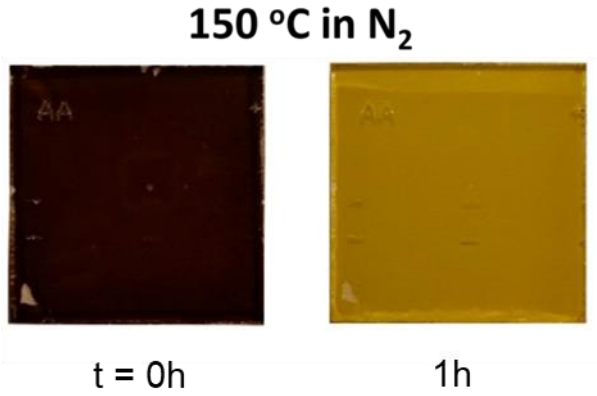


***Figure S30: Thermal stability of a MAPb($I_{0.6}Br_{0.4}$)$_3$ film using the DMF/DMSO anti-solvent quenching method, stressed at 150 °C in a nitrogen atmosphere.*** *Photographs of films measured before and after thermal stressing.*

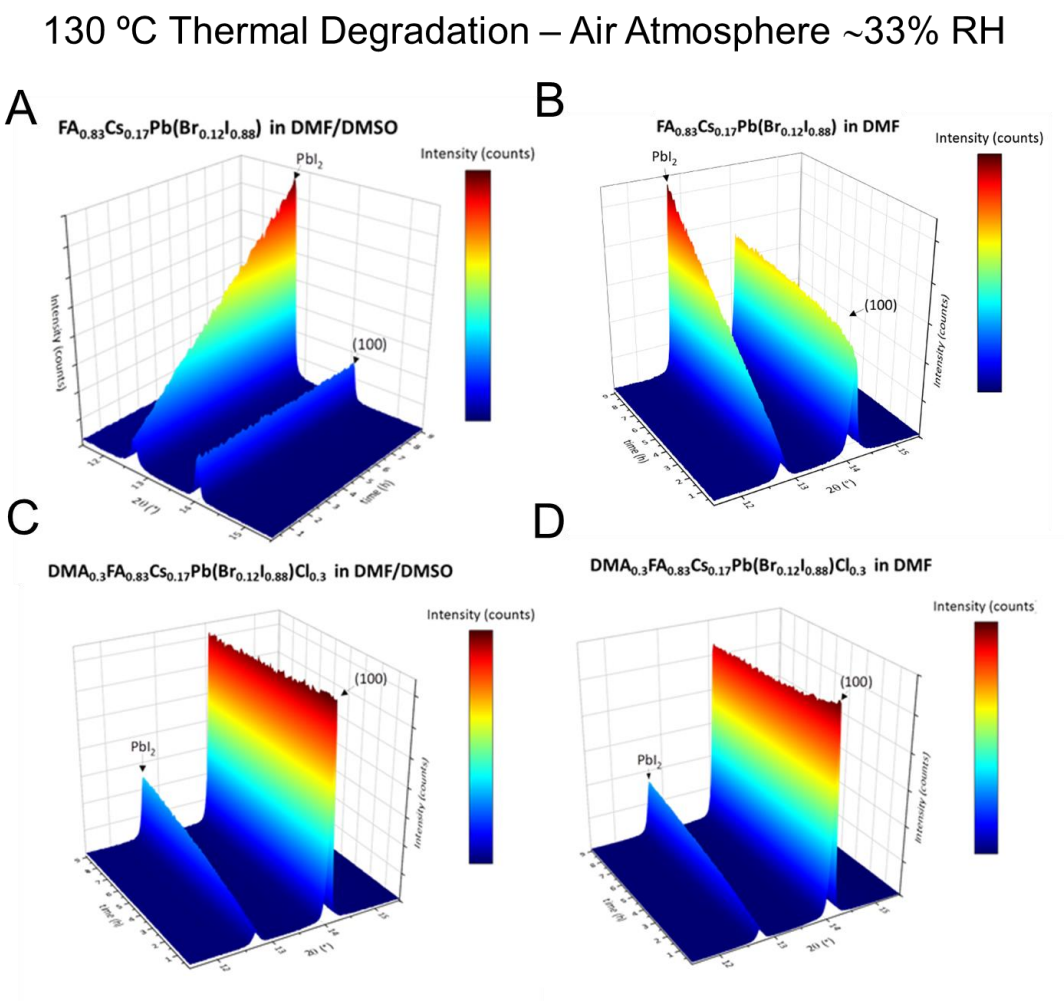


***Figure S31: Evolution of XRD during the thermal degradation of perovskite films at 130 °C in an air atmosphere with ~33% relative humidity.*** *The perovskite films were prepared using A) $FA_{0.83}Cs_{0.17}Pb(Br_{0.12}I_{0.88})_3$ with a DMF/DMSO solvent mixture B) $FA_{0.83}Cs_{0.17}Pb(Br_{0.12}I_{0.88})_3$ with a neat DMF C) $DMA_{0.3}FA_{0.83}Cs_{0.17}Pb(Br_{0.12}I_{0.88})_3Cl_{0.3}$ with a DMF/DMSO solvent mixture D) $DMA_{0.3}FA_{0.83}Cs_{0.17}Pb(Br_{0.12}I_{0.88})_3Cl_{0.3}$ with a neat DMF solvent.*

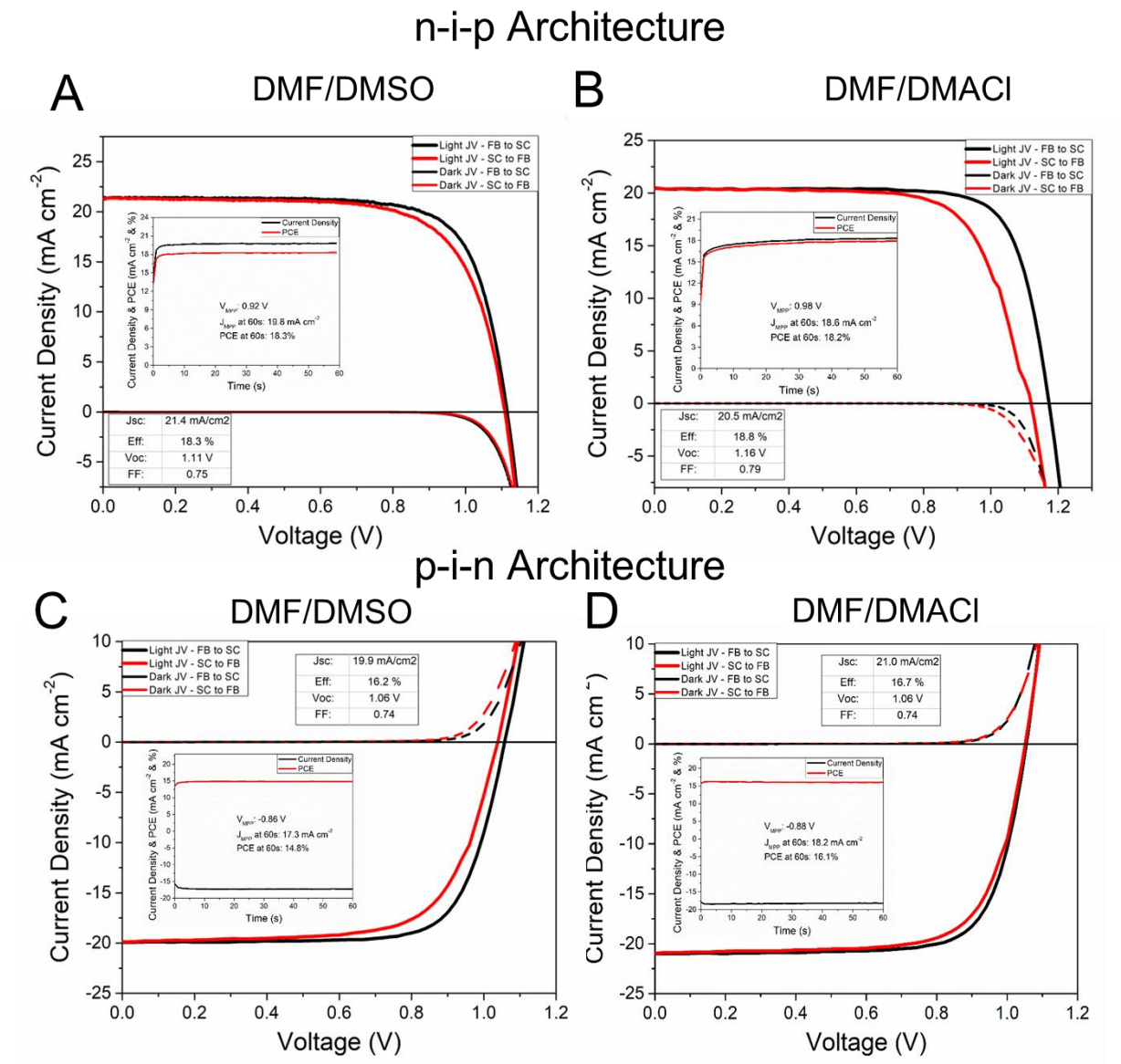


***Figure S32: Performance comparison of perovskite solar cells devices prepared with DMF/DMSO or the DMF/DMACl fabrication method.*** *A, B) J-V characteristics for the champion n-i-p device of DMF/DMSO and DMF/DMACl designs. (Inset) corresponding stabilised PCE and current density measured at the maximum power point. C, D) J-V characteristics for the champion p-i-n devices of DMF/DMSO and DMF/DMACl designs, measured at its peak efficiency.*

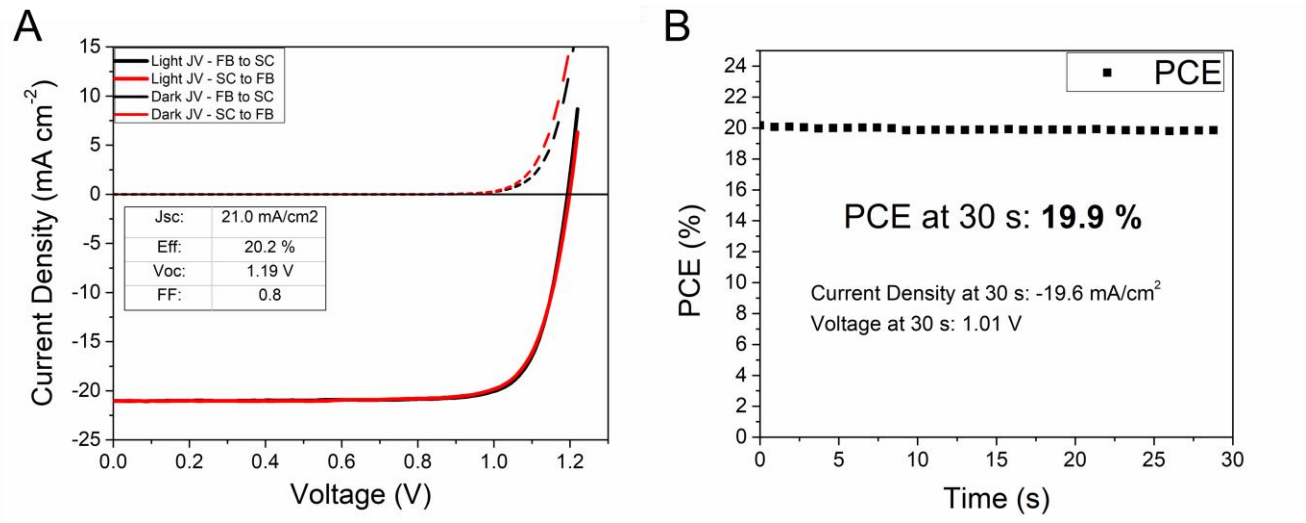


***Figure S33: n-i-p performance of the champion perovskite solar cells devices prepared with DMF/DMACl fabrication method with KCl treatment post-treatment of the $SnO_2$.*** *A) J V characteristics for the champion n-i-p device. B) Corresponding stabilised PCE measured at the maximum power point.*

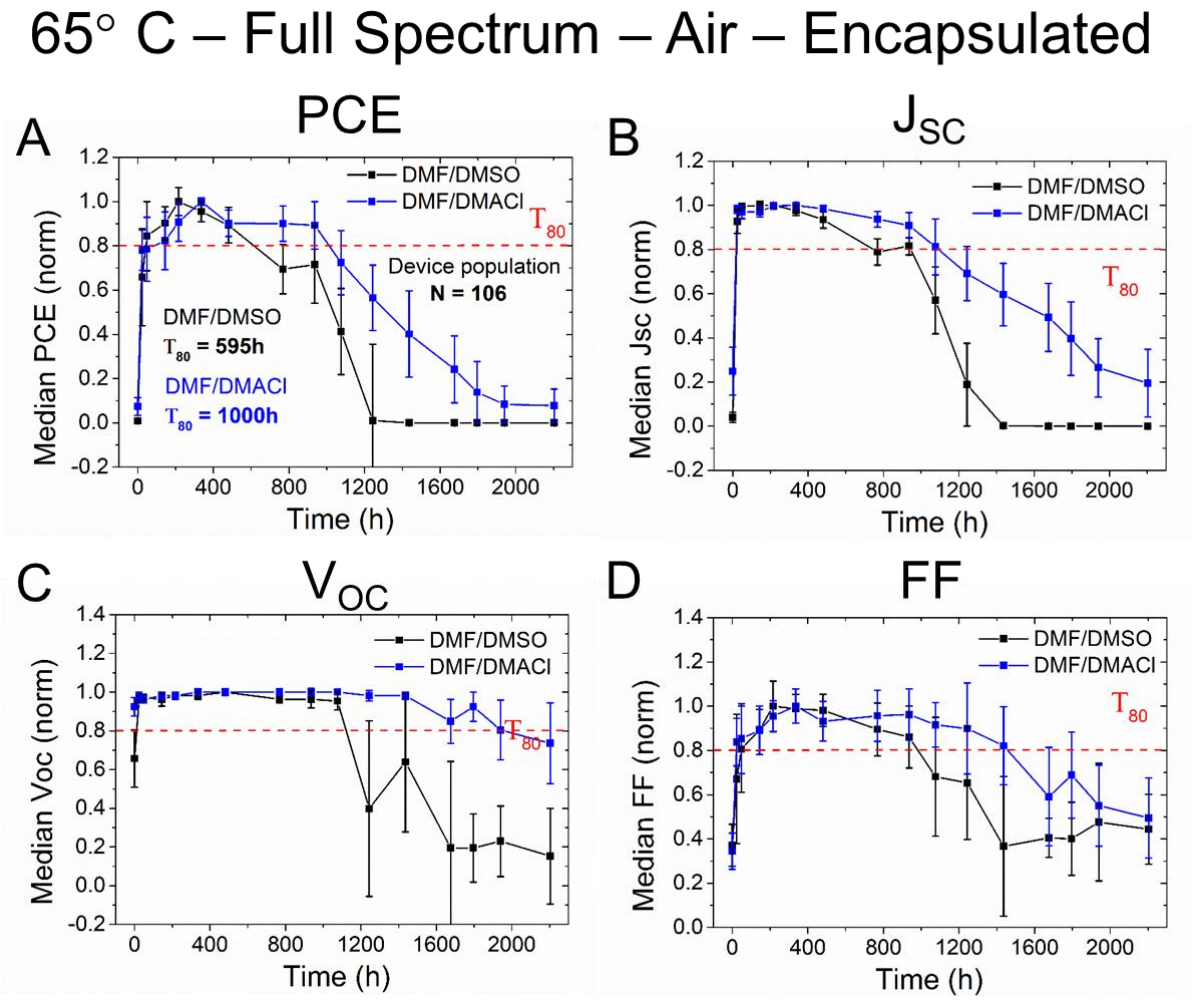


***Figure S34:*** *Evolution of the JV performances between DMF/DMSO and DMF/DMACl fabrication methods under full spectrum simulated AM 1.5, 76 mWcm$^{-2}$ average irradiance at $V_{OC}$ in air without a UV filter at 65 °C, using a Suntest XLS + aging box which irradiates pulsed light. All devices are encapsulated p-i-n devices comprised of a FTO/PTAA/$Al_2O_3$ NPs/perovskite/LiBr/$C_{70}$/Zr(Acac)/PEIE/Au structure. We show the JV characteristics of the A) PCE, B) $J_{SC}$, C) $V_{OC}$ and D) FF. The error bars were calculated using the median absolute deviation (MAD), as a measure of statistical dispersion.*

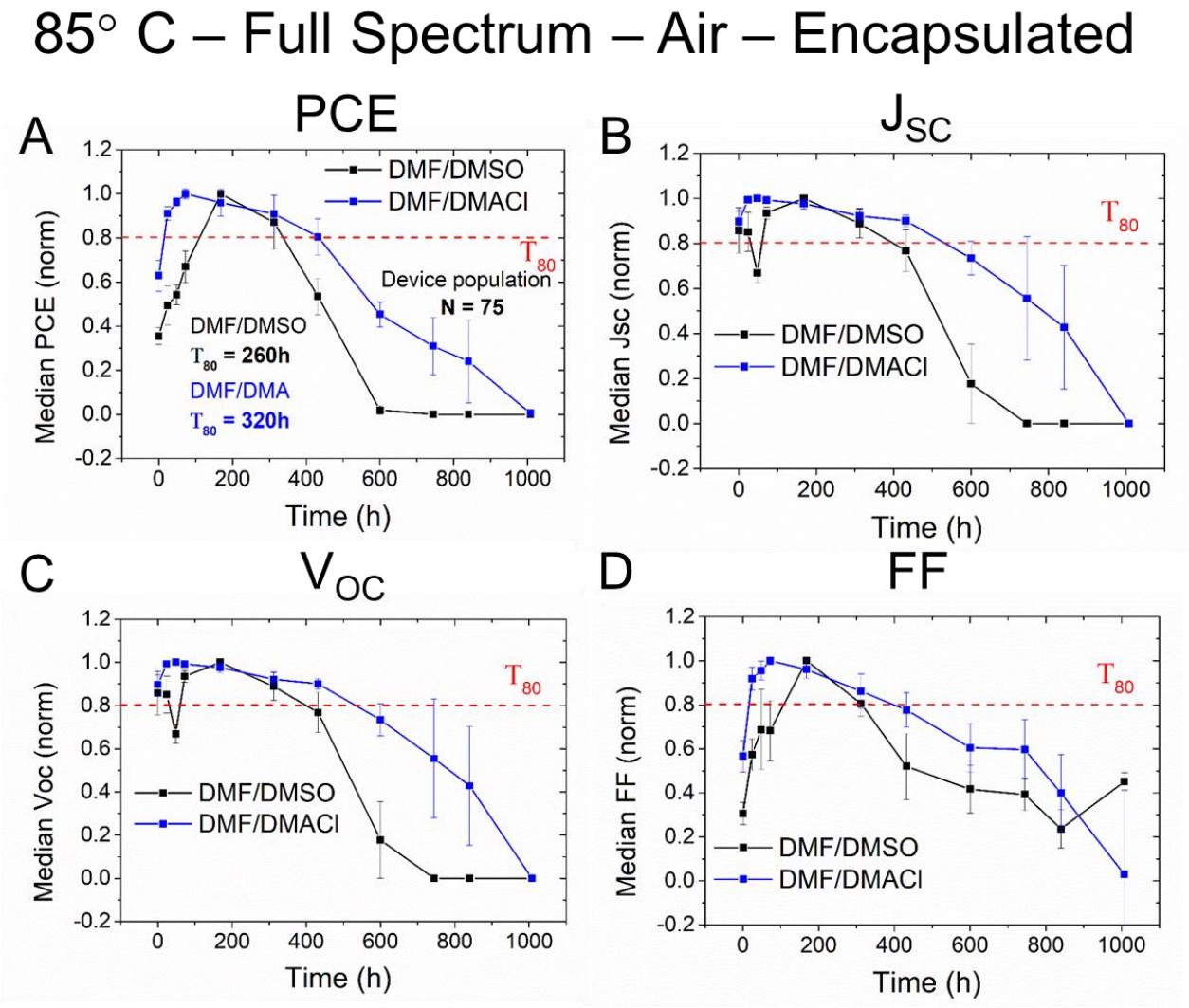


***Figure S35:*** *Evolution of the JV performances between DMF/DMSO and DMF/DMACl fabrication methods under full spectrum simulated AM 1.5, 76 mWcm$^{-2}$ average irradiance at $V_{OC}$ in air without a UV filter at 85 °C, using a Suntest XLS + aging box which irradiates pulsed light. All devices are encapsulated p-i-n devices comprised of a FTO/PTAA/$Al_2O_3$ NPs/perovskite/LiBr/$C_{70}$/Zr(Acac)/PEIE/Au structure. We show the JV characteristics of the A) PCE, B) $J_{SC}$, C) $V_{OC}$ and D) FF. The error bars were calculated using the median absolute deviation as a measure of statistical dispersion.*

# Experimental Section

## Methods

### Fabrication of perovskite devices

## p-i-n devices - Glass/FTO/PTAA/$Al_2O_3$ NPs/perovskite/LiBr/$C_{70}$/$Zr(Acac)_4$/Au

**Substrate Preparation:** Devices were fabricated on fluorine-doped tin oxide (FTO) coated glass (Pilkington, 15Ω/sq). Initially, FTO was removed at specific regions where the anode contact will be deposited. This FTO etching was done using a 2M HCl and zinc powder. Substrates were then cleaned with Hellmanex detergent and rinsed with water. Finally, the substrates were then cleaned sequentially in acetone, isopropyl alcohol (IPA) and dried with nitrogen gun.

**PTAA layer fabrication:** A Poly[bis(4-phenyl)(2,4,6-trimethylphenyl)amine] (PTAA) precursor solution was prepared by dissolving a 1.5 mg $ml^{-1}$ PTAA (Xi'an Polymer) in a 1:1 anhydrous chloroform (CF): chlorobenzene (CB). We spin-coated this solution dynamically in a nitrogen-filled glovebox at 2000 rpm for 20 s and annealed the substrate at 150 °C for 10 mins in air.

**$Al_2O_3$ Nanoparticles (NPs) layer fabrication:** An alumina nanoparticles ($Al_2O_3$ NPs) (< 50 nm) precursor solution was prepared by dispersing an isopropanol (IPA) in 1:150 v/v ratio ($Al_2O_3$ NPs:IPA). A 50 µL of this dispersion was then dynamically spin-coated onto the PTAA layer at 4000 rpm for 30 s. A subsequent anneal of at least 5 min at 85 °C was done.

**DMF/DMSO perovskite precursor solution preparation:**

For the $FA_{0.83}Cs_{0.17}Pb(Br_{0.2}I_{0.8})_3$, the FA/Cs (formamidinium/Cs) perovskite solutions were prepared by dissolving the precursor salts: 171.3 mg FAI (99.99%, GreatCellSolar), 53.0 mg CsI (99.9%, Alfa Aesar), 132.1 mg $PbBr_2$ (98%, Alfa Aesar), 387.2 mg $PbI_2$ (99.99% trace metals and a purity of > 98.0% (T), TCI), in 1 mL of anhydrous N,N-dimethylformamide (DMF): dimethylsulfoxide (DMSO) in a 4:1 v/v ratio to obtain a stoichiometric solution with the desired composition. For fine tuning the Br/I ratio, we varied the ratio of $PbI_2$ to $PbBr_2$ to obtain a precursor solution with the desired halide molecular ratio.

**DMF/DMSO perovskite layer preparation:**

The DMF/DMSO perovskite precursor perovskite solution was spin-coated in a nitrogen-filled using a two-step program. After spreading 50 µL of the perovskite solution onto the substrate, the first step is programmed to spin at 1000 rpm for 10 s. The second step is programmed at 6000 rpm for 20 s. 10 s prior to the end of the second step, 100 µL of ethyl acetate (EA) solvent was dropped on the film. The films were immediately placed on a hotplate in $N_2$ at 100 °C for 20 mins.

**DMF/acid perovskite precursor solution preparation:**

For the $FA_{0.83}Cs_{0.17}Pb(Br_{0.2}I_{0.8})_3$, the FA/Cs (formamidinium/Cs) perovskite solutions were prepared by dissolving the precursor salts: 171.3 mg FAI (99.99%, GreatCellSolar), 53.0 mg CsI (99.9%, Alfa Aesar), 132.1 mg $PbBr_2$ (98%, Alfa Aesar), 387.2 mg $PbI_2$ (99.99% trace metals and a purity of > 98.0% (T), TCI), in 1 mL of anhydrous N,N-dimethylformamide (DMF) to obtain a stoichiometric solution with the desired composition. A 85.6 µl of hydroiodic acid (HI) (57 wt. % in $H_2O$, distilled, stabilized, 99.95%, Sigma-Aldrich) and an 18.4 µl/ml of hydrobromic (HBr) (48 wt. % in $H_2O$) was added for every 1 ml of DMF. After the addition of the acids, the perovskite precursor solution was aged for 48 hours in a nitrogen atmosphere. For fine tuning the Br/I ratio, we varied the ratio of $PbI_2$ to $PbBr_2$, along with the HI to HBr ratio, to obtain a precursor solution to obtain the desired halide molecular ratio.

**DMF/acid perovskite layer preparation:**

The DMF/acid precursor perovskite solution was aged for 48 hours under $N_2$ atmosphere and then spin-coated in a nitrogen-filled glovebox at 2000 rpm for 45s with a 1000 rpm/s ramp rate. The films were dried inside a $N_2$ glovebox on a hot plate at a temperature of 70 °C for 1 minute. The films were then annealed in an oven in an air atmosphere at 185 °C for 90 minutes. During this annealing process, the samples were covered with a large glass container to prevent dust contamination.

**DMF/DMACl perovskite precursor solution preparation:**

For the $DMA_xFA_{0.83}Cs_{0.17}Pb(Br_{0.12}I_{0.88})_3Cl_x$ perovskite solution, we prepared it by dissolving the precursor salts: 199.8 mg FAI, 61.8 mg CsI, X mol % DMACl (e.g. 34.2 mg for X=0.3), 92.5 mg $PbBr_2$, 529.2 mg $PbI_2$, in 1 mL of anhydrous N,N-dimethylformamide (DMF) to obtain a stoichiometric solution with the desired composition. The precursor solution was prepared using the following precursor salts: formamidinium iodide (FAI) (99.99%, GreatCellSolar), caesium iodide (CsI) (99.9%, Alfa Aesar), lead iodide ($PbI_2$) (99.99% trace metals and a purity of > 98.0% (T), TCI), lead bromide ($PbBr_2$) (98%, Alfa Aesar), Dimethylammonium Chloride (DMACl) (≥ 98.0 %, Alfa Aesar). For fine tuning the Br/I ratio, we varied the ratio of $PbI_2$ to $PbBr_2$ to obtain a precursor solution to obtain the desired halide molecular ratio. Similarly, we fine-tuned the DMACl concentration by varying the precursor solution to obtain the desired molecular ratio.

**DMF/DMACl perovskite layer deposition:**

The DMF/DMACl perovskite precursor perovskite solution was spin-coated in a nitrogen-filled glovebox using a two-step program. After spreading 50 µL of the perovskite solution onto the substrate, the first step is programmed to spin at 1000 rpm for 7 s; the second step is programmed at 4000 rpm for 20 s. 5 s

after the start of the second step, 100 µL of a 3:1 α,α,α-Trifluorotoluene (TFT): ethyl acetate (EA) solvent mixture was dropped on the film to quench growth of perovskite. The films were immediately placed on a hotplate in $N_2$ at 100 °C for 5 m. This step is designed to remove the solvent; however, at this point, the perovskite remains in its yellow intermediate phase. A subsequent annealing step on a 170 °C preheated hotplate in air for 10 mins allows for the 2H to 3C sequence to take place, where the films turn from a yellow to a black colour. A last annealed step takes place in a 175 °C preheated oven in air for 90 mins to fully crystallize the perovskite. In the over, a large glass cover lid is placed over the samples to prevent dust particles and airflow from affecting the annealing.

**FABr layer deposition:**

A formamidinium bromide (FABr) precursor solution was prepared by dissolving 2 mg $ml^{-1}$ of FABr (Sigma, (99.99%, GreatCellSolar)) in isopropanol (IPA). After the full crystallization of the perovskite, we spin coated this solution dynamically in a nitrogen-filled glovebox at 4000 rpm for 20 s, and annealed the substrate at 100 °C for 5 min in $N_2$. The FABr solution was dropped within the first 5 s of spin coating. The FABr was deposited on all p-i-n devices of various designs.

**LiBr layer deposition:**

A lithium bromide (LiBr) precursor solution was prepared by dissolving 0.15 mg $ml^{-1}$ of LiBr (Sigma) in isopropanol (IPA). We spin-coated this solution dynamically in a nitrogen-filled glovebox at 4000 rpm for 20 s and annealed the substrate at 85 °C for 10 min in $N_2$.

**$C_{70}$ layer fabrication:**

A $C_{70}$ fullerene precursor solution was prepared by dissolving a 24 mg $ml^{-1}$ of $C_{70}$ (Solenne) in dichlorobenzene (DCB). We spin coated this solution statically in a nitrogen-filled glovebox at 800 rpm for 40 s, on a preheating substrate at 85 °C. We annealed the substrate at 85 °C for 10 min in $N_2$.

**$Zr(Acac)_4$/PEIE layer fabrication:**

A zirconium (IV) acetylacetonate/polyethylenimine ethoxylated ($Zr(Acac)_4$/PEIE) precursor solution was prepared by dissolving a 2 mg $ml^{-1}$ of $Zr(Acac)_4$ (sigma, 97%) in isopropanol (IPA) and adding a 0.1% (v/v) of PEIE (80% ethoxylated solution, 37 wt. % in $H_2O$, Sigma) to this solution. We spin coated this solution dynamically in a nitrogen-filled glovebox at 4000 rpm for 20s.

## n-i-p devices - Glass/FTO/$SnO_2$ CL/$SnO_2$ CBD/KCl/perovskite/PEAI/Spiro/Au

**Substrate Preparation:** Devices were fabricated using fluorine-doped tin oxide (FTO) Tec7 coated glass (Pilkington) as the transparent electrode. FTO was etched with 2 M HCl and zinc powder to obtain the required electrode pattern. Following a cleaning procedure consisting of a series of sonication steps were applied. First 10 min in Decon (5% in deionized water), followed by 10 min of sonication in acetone and finally isopropanol.

**$SnO_2$ Compact Layer (CL):** The substrates were plasma cleaned (Pico, Diener electronic) for 10 min. In the meantime, a $SnCl_2 \bullet 2H_2O$(Alfa Aesar, 99.995%) of 17.5 mg/ml solution in IPA was prepared. Statically 200 ml of the $SnCl_2$ solution were deposited at 3000 rpm (200 acc.) for 25 s in ambient atmosphere (between 30 to 50% RH, 20 to 25 °C). Until all substrates were finished, the substrates were annealed at 100 °C until all substrates were spun and brought onto a sintering hotplate. They were heated with the lid closed and no gas flow attached for 1h at 180 °C.

**$SnO_2$ Compact Bath deposition (CBD):**

We first prepare a bath solution, for 32 substrates (28x28 mm) the following solution was prepared with the compounds: 200 ml of deionised water, a 2.5 g Urea (Sigma-Aldrich), 50 µl Thioglycolic acid (Sigma-Aldrich, 98%), 2.5 ml HCl (99.999%, Alfa Aesar 087617.AK, CAS 7647-01-0), 540 mg $SnCl_2$ (≥99.99%, Sigma-Aldrich, 43508-50g, CAS 10025-69-1). After adding each component, the solution was stirred with a stir bar for a few minutes. We then added the substrates into a glass beaker and filled it with the chemical bath solution and cover it with a glass cover. The substrates were then heated in a ventilated oven at 90 °C for 4 h. After the heating process, the chemical bath was drained, and the glass baker was quickly filled with DI water. Afterwards, the substrates were sonicated for 5 mins in DI, dried with $N_2$ gun and then rinsed with IPA for 5 minutes. Finally, the substrates were heated at 180 °C on a sintering hotplate as previously for 1 h. The substrates were subjected to a UV-Ozone before usage for 15 min.

**KCl Treatment:**

We use 20 mM KCl solution in DI water. We statically spin coated 200 µl of the solution at 3000 rpm (2000 acc.) for 30 s in ambient atmosphere onto the substrate. The substrate was annealed on a hotplate at 100 °C for 10 mins.

**DMF/DMSO perovskite preparation**: $FA_{0.83}Cs_{0.17}Pb(I_{0.88}Br_{0.12})_3$ perovskite 827.86 mg of FAI (99.999%, Dyenamo), 256.17 mg CsI (99.998%, Alfa Aesar), 2192.56 mg of $PbI_2$ (99.999% Alfa Aesar) and 382.16 mg $PbBr_2$ (98%, Alfa Aesar) are dissolved in 4 ml of 4:1 DMF: DMSO. They were stirred at room temperature in the glovebox for 1 to 3 hours before deposition. 70 µl of the solution is spread onto the substrate statically and spin-coated at 10 s at 1000 rpm (200 rpm acc.) and 35 s at 6000 rpm (2000 rpm acc.) and solvent quenched with 150 µl anisole 10 s before the end. The layers were annealed at 100 °C for 15 min. Spinning and heating for the control device were done in a drybox at 20% RH.

**DMF/DMACl perovskite preparation:** $DMACl_{0.3}FA_{0.83}Cs_{0.17}Pb(I_{0.88}Br_{0.12})_3$ perovskite 136.99 DMACl (Sigma-Aldrich), 799.32 mg of FAI (99.999%, Dyenamo), 247.34 mg CsI (99.998% Alfa Aesar), 2117.0 mg of $PbI_2$ (99.999% Alfa Aesar) and 369.9 mg $PbBr_2$ (98%, Alfa Aesar) are dissolved in 4 ml DMF. They are stirred at room temperature in the glovebox for 1 to 3 hours before deposition. 70 µl of the solution is spread onto the substrate statically and spin-coated at 10 s at 1000 rpm (1000 rpm acc.) and 30 s at 4000 rpm (4000 rpm acc.) and solvent quenched with 150 µl TFT 17 s into the program. The layers were annealed at 100 °C for 10 min and directly afterwards at 170 °C. The 30 mol% DMACl:$FA_{0.83}Cs_{0.17}Pb(I_{0.88}Br_{0.12})_3$ perovskite was spun in drybox at 20% RH at around 23 to 25 °C. The heating for the 170 °C step was performed in ambient (30 to 55% RH).

**PEAI layer deposition:**

A phenethylammonium iodide (PEAI) precursor solution was prepared by dissolving 1.25 mg $ml^{-1}$ of PEAI (99.99%, GreatCell Solar) in isopropanol (IPA). After the full crystallization of the perovskite, we spin coated this solution dynamically in a dry air-filled glovebox at 5000 rpm for 20 s, and annealed the substrate at 100 °C for 5 min in a dry air atmosphere. The PEAI solution was dropped within the first 5 s of spin coating.

**Spiro-OMe-TAD preparation:** The hole transfer materials were deposited by preparing a spiro-OMe-TAD in chlorobenzene (90 mg/mL, Lumtech) and mixing with 35.5 uL 4-tert-butyl-pyridine (TBP), 23 uL Li-bis(trifluoromethanesulfonyl)imide (Li-TFSI) (520 mg/mL acetonitrile), and 5 µL tris(2-(1h-pyrazol-1-yl)-4-tert-butylpyridine)-cobalt(III)tris(bis(trifluoromethylsulfonyl)imide) (FK209, Lumtech) (180 mg/mL acetonitrile). The spiro layer was deposited at 4000 rpm for 25 s with 2000 acc in a Drybox at 20% RH.

**Metal electrode layer fabrication:**

An 80 nm gold electrode was thermally evaporated under a vacuum of ≈$10^{-6}$ Torr, at a rate of ≈ 0.2 $nm{\cdot}s^{-1}$ or 0.01 to 0.04 nm/s, respectively.

**Encapsulation:**

A glass/glass encapsulation was sealed with a UV-cured epoxy (LT-U001 UV-Glue, Lumtec). The UV glue was cured for 30 mins with a UV lamp containing 4 x 9W bulbs under $N_2$ atmosphere.

## Measurements

**Wide-angle X-ray scattering (WAXS) measurement:**

Wide-angle X-ray scattering (WAXS) measurement was performed using the Stanford Synchrotron Radiation Lightsource (SSRL) Beamline 11–3 with an X-ray wavelength of 0.9744 Å. Two-dimensional scattering data were collected using a Rayonex MX225 detector in a grazing incidence geometry with the X-ray beam held at an incident angle of 3°. Images are calibrated using a LaB6 standard and integrated between 10° < χ < 170° (χ is the polar angle) using GSAS-II.[3]

**Two-dimensional (2D) X-ray diffraction ($XRD^2$):**

2D-XRD spectra were conducted in ambient air at room temperature using a Rigaku SmartLab X-ray diffractometer with $CuK_{\alpha 1}$ (1.54060 Å) and a HyPix-3000 2D hybrid pixel array detector, operated at 40 kV.

**Nuclear magnetic resonance (NMR):**

$^1$H-NMR spectra were recorded on a Bruker Avance III 400 MHz or 600 MHz spectrometers. For each measurement, 16 perovskite films (2.5x2.5 cm) were scratched off the substrates. The perovskite material was then suspended in deuterated acetonitrile ($CD_3CN$), and the suspension was decanted. All spectra are referenced versus residual solvent peaks with respect to δ(TMS) = 0 ppm.

**Scanning electron microscopy**: The morphology of perovskite films was investigated using a SEM (Hitachi S-4300) at an accelerating voltage of 3-5 kV.

**Solar cell characterization:** The current density–voltage (J-V) curves were measured (2400 Series SourceMeter, Keithley Instruments) under simulated AM 1.5 sunlight at approximately 100 $mWcm^{-2}$ irradiance generated by an Abet Class AAB sun 2000 simulator, with the intensity calibrated with an NREL calibrated KG5 filtered Si reference cell. The mismatch factor was

calculated to be less than 1%. The active area of the solar cell is 0.0919 $cm^{-2}$, by employing an opaque mask with an aperture. The forward J–V scans were measured from forward bias (FB) to short circuit (SC), and the backward scans were from short circuit to forward bias, both at a scan rate of 0.25V $s^{-1}$. A stabilization time of 5 seconds under 1 sun illumination and forward bias of 0.2V above the expected $V_{OC}$ was done prior to scanning.

**External quantum efficiency measurement:**

The external quantum efficiency (EQE) was measured by Fourier-transform photocurrent spectroscopy (FTPS) using each perovskite solar cell as the detector in a Bruker Vortex 80v, and an AM1.5 filtered xenon lamp (Oriel Sol 3A) as the light source. The cells were aged under open-circuit conditions under the AM1.5 spectrum, and the EQE spectra were measured periodically by filtering out above-band-gap illumination to extend the dynamic range of the measurement of the response to sub-band-gap illumination. The measurements were calibrated against the response of a certified Si reference cell (Newport).

**Thermogravimetric analysis (TGA):**

We performed thermogravimetric analysis (TGA) directly on a perovskite-coated glass substrate to preserve and study the morphology of the perovskite. A thin microscope glass coverslip was used as substrate. The choice of a low-weight substrate allowed for an acceptable signal-to-noise ratio for the TGA measurement. A TA Instruments Q500 Thermogravimetric Analyser was used for the measurements of the coatings. This instrument allows the measurement of weight change as a function of temperature/time in a controlled environment. Instrument control was performed using TA Instruments Thermal Advantage software. Subsequent data analysis was performed using TA Instruments Universal Analysis data analysis program. The sample was cut to size and placed inside a 100 ul Platinum crucible (coated side up), and heated at a rate of 10 °C per minute in a controlled atmosphere (Nitrogen) at a flow rate of 100 ml per minute. Precise gas flow control was maintained via a Mass Flow Controller built into the instrument. The mass of the sample was recorded as a function of temperature during the experiment. Data has been plotted to show the relationship between weight and temperature, and also included are the first derivative profiles for the weight losses observed, which give a clear indication of the onset and range of decomposition.

**TOF-SIMS:**

An ION-TOF TOF-SIMS V Time of Flight SIMS (TOF-SIMS) spectrometer was utilized for depth profiling and chemical imaging of the perovskite utilizing methods outlined in detail by Harvey *et.al.*[4]. Analysis was completed utilizing a 3-lens 30kV BiMn primary ion gun. 3-D tomography was completed with 100nm lateral resolution using a $Bi_3^{++}$ primary ion-beam cluster (100 ns pulse width, 0.1 pA pulsed beam current) and a 50x50 µm area was sampled with a 1024:1024 primary

beam raster. Depth Profiling was accomplished with a 1kV oxygen ion sputter beam (5-10 nA sputter current) with a raster of 150×150 microns. After completion of the SIMS measurements, the depth of the craters was determined by optical interference light microscopy in order to convert the SIMS sputter time scale to a sputter depth scale.

**Stability test:**

A glass/glass encapsulation was sealed with a UV-cured epoxy (LT-U001 UV-Glue, Lumtec). The UV glue was cured for 30m with a UV lamp containing 4 x 9W bulbs under $N_2$ atmosphere. All the devices were aged under full spectrum simulated AM1.5G, 76 mW cm$^{-2}$ irradiance at $V_{oc}$ using an Atlas SUNTEST XLS+ (1700W air-cooled Xenon lamp). The chamber temperature was set to °65 or 85 °C. The aging test is in correspondence to ISOS-L-2 aging condition. We note that the light source is pulsed at 100Hz frequency.

**Halide segregation analysis:**

We consider the inflection point of the majority phase EQE to be the bandgap of the majority phase ($E_{g,majority}$), while the bandgap of the minority phase ($E_{g,minority}$) was determined by fitting the sub-bandgap absorption to absorptance modelled via a generalized transfer matrix model.[5] We modelled the optical refractive index $\tilde{n}$ of the halide-segregated perovskite as an effective medium for the two phases, leading to the following expressions:

$$\tilde{n}_{segregated} = \chi \cdot \tilde{n}_{minority} + (1-\chi)\tilde{n}_{majority}$$

Where $\tilde{n}_{segregated}$ is the refractive index of the halide-segregated perovskite, $\tilde{n}_{minority}$ is the refractive index of the minority phase, $\tilde{n}_{majority}$ is the refractive index of the majority phase, and $\chi$ is the molar fraction of the film. We can then model the absorption, $A(E)$, as;

$$A(E) = 1 - e^{-\chi \cdot \alpha_{minority}(E) \cdot t} \approx \chi \cdot \alpha(E) \cdot t$$

Where $\alpha_{minority}$ is the the absorption coefficient of the minority phase $t$ is the film thickness, and $\chi$ is the molar fraction of the film. Additional details are provided in the supplementary information with the assumptions that were made.

We specify that the refractive index of perovskites of different bandgaps is modelled by linearly shifting the extinction co-efficient of $MAPbI_3$ and then performing a Kramers-Kronig transform to obtain the refractive index, following the approach of Hoerantner et al.[6] In our previous work, we have shown that the bandgaps of mixed-halide perovskites do shift linearly in this way.[7] Since the fraction of the minority phase is low (few %), the Bruggeman EMA is, in effect, a linear combination of the two optical constants:

$$\tilde{n}_{segregated} = \chi \cdot \tilde{n}_{minority} + (1-\chi)\tilde{n}_{majority}$$

With the Beer-Lambert approximation, the absorptance $A$ can be written as:

$$A(E) = 1 - e^{-(\chi \cdot \alpha_{minority} + (1-\chi) \cdot \alpha_{majority}) \cdot t}$$

Here $\alpha$ is the absorption coefficient and $t \sim 500\,nm$ is the film thickness. In the region where only the minority phase absorbs, we can write:

$$A(E) = 1 - e^{-\chi \cdot \alpha_{minority}(E) \cdot t} \approx \chi \cdot \alpha(E) \cdot t$$

The approximation is valid since $e^x - 1 \approx x$ for $x \ll 1$. To calculate $\chi$, we evaluate this expression at $E = E_{g,minority.}$

Detailed balance calculations in the radiative limit were used to evaluate the change in open-circuit voltage upon halide-segregation.[8–10] The Urbach tails of the measured EQEs were extrapolated to 1.2 eV and above 1.76 eV. The calculation assumes that the radiative efficiency of the cell does not change upon segregation. As carrier funnelling is likely to increase the radiative efficiency, the calculated $V_{OC}$ loss is an upper bound.

## References


[1] G. Widmann, **n.d.**

[2] Thass, "Buoyancy Phenomenon in TGA Systems," can be found under http://thass.net, **n.d.**

[3] B. H. Toby, R. B. Von Dreele, *J. Appl. Crystallogr.* **2013**, *46*, 544.

[4] S. Braunger, L. E. Mundt, C. M. Wolff, M. Mews, C. Rehermann, M. Jost, A. T. ESTEVES, D. Eisenhauer, C. Becker, J. A. G. Torres, E. Unger, L. Korte, D. Neher, M. C. Schubert, B. Rech, S. Albrecht, *J. Phys. Chem. C* **2018**, *122*, 17123.

[5] E. Centurioni, *Appl. Opt.* **2005**, *44*, 7532.

[6] M. T. Hörantner, T. Leijtens, M. E. Ziffer, G. E. Eperon, M. G. Christoforo, M. D. McGehee, H. J. Snaith, *ACS Energy Lett.* **2017**, *2*, 2506.

[7] D. P. McMeekin, G. Sadoughi, W. Rehman, G. E. Eperon, M. Saliba, M. T. Hörantner, A. Haghighirad, N. Sakai, L. Korte, B. Rech, M. B. Johnston, L. M. Herz, H. J. Snaith, *Science* **2016**, *351*, 151.

[8] S. Mahesh, J. M. Ball, R. D. J. Oliver, D. P. McMeekin, P. K. Nayak, M. B. Johnston, H. J. Snaith, *Energy Environ. Sci.* **2020**, *13*, 258.

[9] P. K. Nayak, S. Mahesh, H. J. Snaith, D. Cahen, *Nat. Rev. Mater.* **2019**, *4*, 269.

[10] J. F. Guillemoles, T. Kirchartz, D. Cahen, U. Rau, *Nat. Photonics* **2019**, *13*, 501.